JOURNAL OF GEOPHYSICAL RESEARCH, VOL. 96, NO. B1, PAGES 551–577, JANUARY 10, 1991

Large-Scale Three-Dimensional Even-Degree Structure of the Earth From Splitting of Long-Period Normal Modes

XIANG-DONG LI,[1] DOMENICO GIARDINI,[2] AND JOHN H. WOODHOUSE[3]

Department of Earth and Planetary Sciences, Harvard University, Cambridge, Massachusetts

Spectra of the Earth's free oscillations, which depart significantly from those predicted for spherically symmetric Earth models, contain important information on the large-scale aspherical structure of the Earth. In this paper we present theory, techniques, and numerical results for retrieval of Earth models (including mantle heterogeneity, topography of the core-mantle boundary (CMB), and inner core anisotropy), using such data. The inversions for Earth models in this study are based upon spectral splitting of 33 isolated multiplets, observed in long-period accelerograms of 10 large events recorded by the International Deployment of Accelerometers network. Approximately 1000 spectra are involved. Although the data set is insufficient to yield independent results for perturbations in P velocity, S velocity, and density, it is demonstrated that it is possible to obtain large-scale (spherical harmonic degrees $s = 0, 2, 4$) models of mantle heterogeneity from such a data set under the constraint that aspherical perturbations in seismic velocities and density are proportional to one another. The mantle models developed from modal data are remarkably similar to preexisting models based upon other kinds of seismic data, demonstrating that heterogeneity in seismic velocities is, at most, weakly dependent on frequency. The pattern of the inferred CMB topography is consistent with geodynamic predictions and agrees to a fair extent with results based on travel time anomalies of PcP and PKP, indicating that modal data can add independent constraints on CMB topography. The anomalous splitting of core modes is attributed to inner core anisotropy which is assumed to possess cylindrical symmetry about the Earth's rotation axis. We consider a relatively simple model which varies smoothly with radius (only with radially constant terms and terms varying with r^2). Theoretically, 14 parameters are required to describe such an anisotropic tensor field if it is restricted to spherical harmonic degrees 2 and 4 and if analyticity of the field is required. The inversion for such an anisotropic inner core yields a model which can explain the splitting of anomalously split modes, without violating the constraints imposed by $PKIKP$ travel time information. We solve the inverse problem by following two approaches: (1) using splitting function coefficients as data, we derive Earth models by solving linear inverse problems for each spherical harmonic degree and order; and (2) we directly solve the nonlinear inverse problem in which the data are observed modal spectra and the unknowns are the structural parameters. The second procedure has advantages in the case that there are insufficient data to obtain stable results for the splitting functions of some modes. The mantle models generated in these two ways are essentially identical, verifying that splitting functions can serve as a very convenient intermediate stage in modeling Earth structure using the split spectra of free oscillations.

1. INTRODUCTION

In recent years a number of seismological studies, using a variety of different kinds of data, have yielded important information on the Earth's large-scale three-dimensional structure. All regions of the Earth's interior, from the surface to the center, have been touched by these studies, which have been based on seismic data ranging in frequency from approximately 1 Hz to 0.5 mHz. For recent reviews and references to the literature, see *Lay* [1987], *Dziewonski and Woodhouse* [1987], and *Woodhouse and Dziewonski* [1989]. The aim of the present study is to construct Earth models consistent with the observed spectral splitting of a number of free oscillation multiplets.

Spectral splitting is caused by departures of the Earth from spherical symmetry, including rotation, ellipticity, lateral variations in wave speeds and density, anisotropy, and boundary undulations. In general, the properties of a given free oscillation multiplet depend simultaneously upon all such asphericities in all regions of the Earth. In this respect the information derived from free oscillations differs from that provided by other kinds of data, such as the travel times of body waves or the phase delays of surface waves, which depend upon only a restricted set of parameters in restricted geographical regions. While this property of free oscillation data complicates the analysis and interpretation, it may also be seen as an advantage, since it means that results derived from free oscillations are much less affected by shortcomings of the source and station distributions, which plague other methods of tomography. Lasting several days after an earthquake, the standing waves of free oscillation sample the Earth quite uniformly. Since the wavelengths associated with free oscillations are comparable with the Earth's radius, they yield observables which are directly sensitive to the large-scale features of Earth structure.

The splitting of normal modes may be modeled by using the concept of the splitting function [*Woodhouse and Giardini*, 1985], which serves as an intermediate stage in mapping

[1]Now at Seismological Laboratory, California Institute of Technology, Pasadena.

[2]Now at Department of Earth Sciences, Oxford University, Oxford, England.

[3]Now at Istituto Nazionale di Geofisica, Rome, Italy.

Paper number 90JB02009.
0148-0227/91/90JB-02009$05.00

the Earth's interior. The theory and technique for retrieving splitting functions have been described by *Giardini et al.* [1988] (hereinafter referred to as paper 1), who report the inversion results for the low-degree (spherical harmonic degrees $s = 0, 2, 4$) splitting function coefficients of 27 modes. *Ritzwoller et al.* [1988] have also retrieved low-degree "interaction coefficients" (equivalent to the splitting functions) of 37 modes, based on a similar technique and the same kind of data. As attempts to interpret the splitting functions retrieved in these studies, some preliminary mantle models have been reported [*Giardini et al.*, 1987; *Ritzwoller et al.*, 1988]. In this paper we give a more complete account of the theory, methods, and assumptions used in constructing such models, together with numerical results for the model parameters and resolution and error analyses.

In this study we adopt two approaches to the retrieval of structural parameters consistent with the modal observations. First, we make use of the splitting coefficients of the 26 multiplets retrieved in paper 1, together with the coefficients of seven newly studied modes presented here, to formulate the linear inverse problem for aspherical perturbations in Earth structure. Because the inverse problem is linear and because it decouples into separate inverse problems for each spherical harmonic degree and order, this approach is a simple and a natural one. It has the disadvantage, however, that the resolution of the splitting functions varies from mode to mode, and thus there is a variable bias in the coefficients, the effects of which are difficult to quantify. We therefore develop a second approach in which we seek Earth models which optimally fit the observed modal spectra, eliminating the intermediate stage of estimating the splitting coefficients. This is a nonlinear inverse problem in which all structural parameters are simultaneously determined, using the spectra of all available multiplets. We find that these two approaches yield very much the same results for the mantle but that the second approach identifies some core modes for which the splitting coefficients are seriously biased. An outcome of the second approach is a set of splitting coefficients for each multiplet subjected to the requirement that they all be consistent with a single structural model. Since linear inverse problems are simpler and allow straightforward estimation of error and resolution, the first approach would certainly be more desirable if the data set were sufficient to yield well-resolved splitting coefficients for all multiplets. With the current data set, however, the second approach is also valuable.

The multiplets used in this study, which have periods ranging from 193 s to 2134 s, may be naturally partitioned into two subsets: "mantle modes" whose splitting behavior can be well explained by the aspherical structure in the mantle and "core modes" whose splitting functions are dominated by zonal patterns which cannot be accommodated in the mantle.

The current data for mantle modes are not sufficient to yield independent results for mantle P velocity (α), S velocity (β), and density (ρ), and we therefore make the assumption that aspherical perturbations in these quantities are proportional ($\delta \ln \alpha \propto \delta \ln \beta \propto \delta \ln \rho$) and assume that the constants of proportionality do not vary with depth. The issue of estimating the proportionality coefficients $d \ln \beta / d \ln \alpha$, $d \ln \rho / d \ln \beta$, has been discussed in a separate contribution (X.-D. Li, D. Giardini, and J. H. Woodhouse, submitted manuscript, 1990). There it is found, by comparing modal splitting coefficients with the predictions of P and S velocity models based on other kinds of data, that $d \ln \beta / d \ln \alpha$ in the lower mantle lies in the interval (1.7, 2.6) with 75% confidence. In this study we adopt the value $d \ln \beta / d \ln \alpha = 2.0$. Since the modal data are relatively insensitive to density, it is found that the value of $d \ln \rho / d \ln \alpha$ is not strongly constrained and for the same reason the results of the present study are not very sensitive to the value of this ratio. Here we adopt the value $d \ln \rho / d \ln \alpha = 0.5$, based upon the experimental results of *Anderson et al.* [1968]. Under these assumptions and ignoring possible mantle anisotropy, mantle structure is modeled in terms of a sixth-order polynomial in depth and for spherical harmonic degrees 0, 2 and 4. The resulting models are found to be in good agreement with results obtained by other authors using different kinds of seismic data.

In the inversion we also include the topography of the core-mantle boundary (CMB) as an unknown. The results show that study of the splitting of normal modes can provide independent constraints on the problem of CMB topography, although the trade-off between the volumetric heterogeneity of the mantle and the CMB structure is severe for the current data set.

A number of modes sensitive to the deep structure of the core display the phenomenon of "anomalous splitting" [*Masters and Gilbert*, 1981; *Giardini et al.* 1987, 1988; *Ritzwoller et al.* 1988], owing to the presence of large zonal terms in their splitting functions. It has been proposed that such anomalous splitting is caused by anisotropy of the material of the inner core [*Woodhouse et al.* 1986], which is also supported by evidence from studies of *PKIKP* travel time anomalies [*Morelli et al.*, 1986; *Shearer et al.*, 1988]. The original studies in which inner core anisotropy was proposed considered the simplest anisotropic inner core model which leads to zonal terms in the splitting functions of core modes, namely, uniform transverse isotropy in the plane of the equator; it was shown, however, that while this model is fairly effective in separately modeling the modal observations and the travel time observations, it is not possible to obtain a model of this kind which simultaneously explains both types of data. It was pointed out that both kinds of data favor, to a first approximation, a cylindrically symmetric distribution of anisotropy, in which the symmetry axis coincides with the Earth's rotation axis. Although the data sets do not adequately constrain all of the parameters upon which a zonal fourth rank elastic tensor field can depend, we derive in this study an inner core anisotropic elastic tensor field, of a relatively simple form, which is consistent with both the modal data and the information from *PKIKP* travel time anomalies.

2. THEORETICAL FRAMEWORK

Knowing the source mechanisms of a number of earthquakes and the instrumental responses of the seismometers, observed seismograms depend solely upon the structure of the Earth, and thus they constitute data which may be used to investigate such structure. In this section we develop the theoretical results relating observed seismic spectra to aspherical model perturbations about a spherically symmetric reference model.

2.1. *Normal Mode Formulation*

Throughout this paper we work under the assumption that we may separate the contribution of an isolated mul-

tiplet from the effects of the neighboring multiplets in frequency domain; i.e., we neglect quasi-degenerate coupling between multiplets [*Dahlen*, 1969; *Luh*, 1973, 1974; *Woodhouse*, 1980]. In first-order degenerate perturbation theory [*Dahlen*, 1968, 1974; *Woodhouse and Dahlen*, 1978], the effect on a multiplet (on its eigenfrequencies and eigenfunctions) of an aspherical perturbation from a spherical reference Earth model is fully described by the splitting matrix of the mode. Following *Woodhouse and Girnius* [1982], the contribution to a seismogram corresponding to a particular isolated multiplet, of angular order l, can be written, as function of time t

$$u(t) = \mathrm{Re}\{\exp(i\omega t)\mathbf{r} \cdot \exp(i\mathbf{H}t) \cdot \mathbf{s}\} \tag{1}$$

where $\mathbf{r}$ and $\mathbf{s}$ are the "receiver vector" and "source vector", respectively, and ω is the complex reference frequency of the multiplet. These are calculated for a reference Earth model. We adopt the preliminary reference Earth model (PREM) of *Dziewonski and Anderson* [1981] as the reference model in this study. The splitting matrix $\mathbf{H}$ is a $(2l+1) \times (2l+1)$ complex matrix with elements $H_{mm'}$, which can be expressed

$$H_{mm'} = m\Omega\beta\delta_{mm'} + \omega_0 \sum_{\substack{s=0 \\ s\ \mathrm{even}}}^{2l} \sum_{t=-s}^{s} \gamma_{st}^{mm'} c_{st} \tag{2}$$

with $\omega_0 = \mathrm{Re}(\omega)$ and

$$\gamma_{st}^{mm'} = (2l+1)\left(\frac{2s+1}{4\pi}\right)^{1/2} (-1)^m \begin{pmatrix} l & l & s \\ -m & m' & t \end{pmatrix} \times \begin{pmatrix} l & l & s \\ 0 & 0 & 0 \end{pmatrix} \tag{3}$$

where the Wigner 3-j symbols [*Edmonds*, 1960] have been introduced. The first term on the right side of (2) is the effect due to the rotation of the Earth, Ω is the Earth's rotational angular velocity, and β is the Coriolis splitting parameter of the multiplet [*Dahlen*, 1968]. The splitting function coefficients c_{st} are linearly related to the perturbations of the reference Earth model. We may write

$$c_{st} = \delta_{s2}\delta_{t0} c^{ell} + \int_0^a \mathbf{M}_s(r) \cdot \delta\mathbf{m}_{st}(r) dr + \sum_d H_s^d \delta h_{st}^d \tag{4}$$

where δ_{ij} is the Kronecker delta. The first term on the right side is the known, theoretical contribution from the Earth's hydrostatic ellipticity of figure [*Dahlen*, 1968, 1976; *Woodhouse and Dahlen*, 1978]; c^{ell} is given in terms of the ellipticity splitting parameter of the multiplet by equation (9) of paper 1. The quantities $\delta\mathbf{m}_{st}$ represent the spherical harmonic coefficients of the volumetric perturbations in elastic property and density form the spherical isotropic Earth model. δh_{st} are the spherical harmonic coefficients of the undulation of the dth boundary. The corresponding kernels $\mathbf{M}_s$ and H_s^d may be calculated in terms of the parameters and eigenfunctions of the reference model; expressions for these are obtainable from the literature. Here we introduce certain specific sets of quantities $\delta\mathbf{m}_{st}$ and δh_{st}^d and summarize the results needed for the current study.

2.2. *Differential Kernels*

Kernels for isotropic heterogeneity. When elastic anisotropy of the Earth is neglected volumetric perturbations $\delta\mathbf{m}_{st}$ in (4) may be characterized, as often in the literature, by heterogeneity in shear modulus ($\delta\mu_{st}$), bulk modulus ($\delta\kappa_{st}$), and density ($\delta\rho_{st}$). However we choose, for convenience in comparison with propagating wave approaches, the relative perturbations in P velocity α, S velocity β, and density ρ to describe the heterogeneity, i.e.,

$$\delta\mathbf{m}_{st}(r) = (\delta\alpha_{st}/\alpha, \delta\beta_{st}/\beta, \delta\rho_{st}/\rho) \tag{5}$$

where the denominators are evaluated in the spherical reference model and the numerators are the spherical harmonic components of degree s and order t of the perturbations. The perturbations in P and S velocities may be complex in order to incorporate attenuation differing from that of the reference model. Correspondingly, the kernel $\mathbf{M}_s(r)$ can be written

$$\mathbf{M}_s(r) = (A_s(r), B_s(r), R_s(r)) \tag{6}$$

Expressions for $A_s(r), B_s(r)$, and $R_s(r)$ in terms of eigenfunctions of the multiplet in the reference model may be calculated from equations (97) and (110)–(112) of *Woodhouse and Dahlen* [1978]. After some straightforward algebra, we obtain

$$\begin{aligned} \omega_0 A_s(r) &= 2r^2\alpha^2\rho K_s \\ &= 2r^2(\kappa + \tfrac{4}{3}\mu)K_s \end{aligned} \tag{7}$$

$$\begin{aligned} \omega_0 B_s(r) &= 2r^2\beta^2\rho(M_s - \tfrac{4}{3}K_s) \\ &= 2r^2\mu(M_s - \tfrac{4}{3}K_s) \end{aligned} \tag{8}$$

and

$$\begin{aligned} \omega_0 R_s(r) &= r^2\rho[(\alpha^2 - \tfrac{4}{3}\beta^2)K_s + \beta^2 M_s + R_s^{(2)}] \\ &= r^2(\kappa K_s + \mu M_s + \rho R_s^{(2)}) \end{aligned} \tag{9}$$

where the kernels K_s, M_s, and $R_s^{(2)}$ are those given by equations (100), (102), and (110) of *Woodhouse and Dahlen* [1978] respectively; κ is the bulk modulus and μ is the shear modulus of the reference model.

Kernels for anisotropy. When elastic anisotropy of the Earth is considered, $\delta\mathbf{m}_{st}$ in (4) may be expressed

$$\delta\mathbf{m}_{st} = (\delta\rho_{st}/\rho, \delta\bar{\mathbf{m}}_{st}) \tag{10}$$

where $\delta\rho_{st}/\rho$ are the relative perturbations in density and $\delta\bar{\mathbf{m}}_{st}$ represent elastic anisotropy perturbations (including perturbations in shear modulus μ and bulk modulus κ).

Mochizuki [1986] has given explicit expressions for the coupling effects of anisotropy in terms of spherical harmonic coefficients of 21 independent contravariant components of an elastic tensor field. Here we show, however, that only 13 independent combinations of these contribute in the case of splitting (i.e. self-coupling). It is convenient, therefore, to decompose the elastic tensor perturbations into two parts: one belonging to the subspace which does not contribute to splitting and the other belonging to the orthogonal subspace.

The splitting matrix elements of a particular mode due to a general elastic tensor $\mathbf{L}$ can be written [*Woodhouse and Dahlen*, 1978]

$$H_{mm'} = \frac{1}{2\omega_0} \int [\nabla\mathbf{u}_{m'} : \mathbf{L} : \nabla\mathbf{u}_m^*] dV \tag{11}$$

where $\mathbf{u}_m (m = -l, \ldots, 0, \ldots, l)$ are the displacement eigenfunctions of the $(2l+1)$ singlets and are subject to the orthogonality relation: $\int \rho \mathbf{u}_m^* \cdot \mathbf{u}_{m'} dv = \delta_{mm'}$, with asterisk denoting complex conjugation, and the volume integration is taken over the whole volume of the Earth. For a multiplet of angular order l, the basis eigenfunctions $\mathbf{u}_m$ are of the form

$$\mathbf{u}_m = U Y_l^m \hat{\mathbf{r}} + V \nabla_1 Y_l^m + W(-\hat{\mathbf{r}} \times \nabla_1 Y_l^m) \tag{12}$$

where Y_l^m denote the surface spherical harmonic of degree l and order m, as defined by *Edmonds* [1960]; U, V, and W are functions of radius r and characterize the eigenfunction of the mode (U and V vanish for a toroidal mode; W vanishes for a spheroidal mode); $\nabla_1 \equiv \hat{\theta}\partial_\theta + \csc\theta\, \hat{\phi}\partial_\phi$; and $\hat{\mathbf{r}}$, $\hat{\theta}$, $\hat{\phi}$ are unit vectors in the spherical coordinate directions.

The general, fourth rank, elastic tensor $\mathbf{L}$ can be expanded in terms of generalized spherical harmonics [*Phinney and Burridge*, 1973]:

$$\mathbf{L} = \sum_{\alpha\beta\gamma\delta} \sum_{s=0}^{\infty} \sum_{t=-s}^{s} L_{st}^{\alpha\beta\gamma\delta} \hat{Y}_s^{Nt} \mathbf{e}_\alpha \mathbf{e}_\beta \mathbf{e}_\gamma \mathbf{e}_\delta \tag{13}$$

where $L_{st}^{\alpha\beta\gamma\delta}$ ($\alpha, \beta, \gamma, \delta$ take values -1, 0, 1) are the coefficients characterizing tensor $\mathbf{L}$, $\mathbf{e}_\alpha$ are complex basis vectors as defined by equation (1.4) of *Phinney and Burridge* [1973], $\hat{Y}_s^{Nt}$ (with $N = \alpha+\beta+\gamma+\delta$) are the generalized spherical harmonics normalized so that

$$\int \hat{Y}_s^{Nt} (\hat{Y}_{s'}^{Nt'})^* d\Omega = \delta_{ss'}\delta_{tt'} \tag{14}$$

where the integration is taken over the surface of the sphere. The generalized spherical harmonics used here are related to Y_s^{Nt} defined by *Phinney and Burridge* [1973] through

$$\hat{Y}_s^{Nt}(\theta, \phi) = \left(\frac{2s+1}{4\pi}\right)^{\frac{1}{2}} Y_s^{Nt}(\theta, \phi) \tag{15}$$

The expansion of $\mathbf{L}$ in terms of generalized spherical harmonics enable us to rewrite (11)

$$\begin{aligned} H_{mm'} &= \frac{1}{2\omega_0} \sum_{\substack{s=0 \\ s \text{ even}}}^{2l} \sum_{t=-s}^{s} \gamma_{st}^{mm'} \int_0^a \sum_{\alpha\beta\gamma\delta} L_{st}^{\alpha\beta\gamma\delta}(r) \\ &\times \varepsilon^{-\alpha-\beta} \varepsilon^{-\gamma-\delta} \xi_{sl}^{(\alpha+\beta)(\gamma+\delta)} r^2 dr \end{aligned} \tag{16}$$

where the integration is taken from the center ($r=0$) to the surface ($r=a$) of the Earth; α, β, γ, δ take values -1, 0, 1; $\varepsilon^{\alpha\beta}$ are symmetric (i.e., $\varepsilon^{\alpha\beta} = \varepsilon^{\beta\alpha}$) and are given by

$$\varepsilon^{\pm 1 \pm 1} = \Omega_0^l \Omega_2^l r^{-1}(V \pm iW) \tag{17}$$

$$\varepsilon^{00} = \dot{U} \tag{18}$$

$$\varepsilon^{+1-1} = -\frac{1}{2} r^{-1}[2U - l(l+1)V] \tag{19}$$

$$\varepsilon^{0\pm 1} = \frac{1}{2}\Omega_0^l [\dot{V} + r^{-1}(U - V) \pm i(\dot{W} - r^{-1}W)] \tag{20}$$

with $\Omega_N^l \equiv [(l+N)(l-N+1)/2]^{\frac{1}{2}}$, and overdot denotes differentiation with respect to r. Finally, the coefficients $\xi_s^{(\alpha+\beta)(\gamma+\delta)}$ in (16) are dimensionless constants defined as follows:

$$\xi_s^{N_1 N_2} = (-1)^{N_1+N_2} \begin{pmatrix} l & l & s \\ -N_2 & -N_1 & N_1+N_2 \end{pmatrix} \Big/ \begin{pmatrix} l & l & s \\ 0 & 0 & 0 \end{pmatrix} \tag{21}$$

Equation (16) indicates that $L_{st}^{\alpha\beta\gamma\delta}$ with s odd have no effect on the splitting. This can be verified by using the symmetry property $L_{st}^{\alpha\beta\gamma\delta} = L_{st}^{\gamma\delta\alpha\beta}$, in addition to the properties of the Wigner 3-j symbols.

Comparison of (2) with (16) leads to

$$c_{st} = \frac{1}{2\omega_0^2} \int_0^a \sum_{\alpha\beta\gamma\delta} L_{st}^{\alpha\beta\gamma\delta} g_s^{\alpha\beta\gamma\delta} r^2 dr \tag{22}$$

where

$$g_s^{\alpha\beta\gamma\delta} = \varepsilon^{-\alpha-\beta} \varepsilon^{-\gamma-\delta} \xi_s^{(\alpha+\beta)(\gamma+\delta)} \tag{23}$$

It is easily verified that for even s the relation

$$g_s^{\alpha\beta\gamma\delta} = g_s^{-\alpha-\beta-\gamma-\delta} \tag{24}$$

holds for both spheroidal and toroidal modes. Therefore (22) can be written in the form

$$c_{st} = \frac{1}{2\omega_0^2} \int_0^a \sum_{\alpha\beta\gamma\delta} \frac{1}{2}(L_{st}^{\alpha\beta\gamma\delta} + L_{st}^{-\alpha-\beta-\gamma-\delta}) g_s^{\alpha\beta\gamma\delta} r^2 dr \tag{25}$$

Any tensor $L^{\alpha\beta\gamma\delta}$ may be decomposed into two parts

$$L^{\alpha\beta\gamma\delta} = \Lambda^{\alpha\beta\gamma\delta} + \bar{\Lambda}^{\alpha\beta\gamma\delta} \tag{26}$$

such that

$$\Lambda^{\alpha\beta\gamma\delta} = \sum_{s,t} \frac{1}{2}(L_{st}^{\alpha\beta\gamma\delta} + L_{st}^{-\alpha-\beta-\gamma-\delta}) \hat{Y}_s^{Nt} \tag{27}$$

and

$$\bar{\Lambda}^{\alpha\beta\gamma\delta} = \sum_{s,t} \frac{1}{2}(L_{st}^{\alpha\beta\gamma\delta} - L_{st}^{-\alpha-\beta-\gamma-\delta}) \hat{Y}_s^{Nt} \tag{28}$$

where $N = \alpha+\beta+\gamma+\delta$. With the above decomposition of $\mathbf{L}$, (25) becomes

$$c_{st} = \frac{1}{2\omega_0^2} \int_0^a \sum_{\alpha\beta\gamma\delta} \Lambda_{st}^{\alpha\beta\gamma\delta} g_s^{\alpha\beta\gamma\delta} r^2 dr \tag{29}$$

The tensor $\bar{\Lambda}$ does not contribute to splitting. The symmetry properties of Λ are given by:

$$\Lambda_{st}^{\alpha\beta\gamma\delta} = \Lambda_{st}^{\beta\alpha\gamma\delta} = \Lambda_{st}^{\gamma\delta\alpha\beta} = \Lambda_{st}^{-\alpha-\beta-\gamma-\delta} \tag{30}$$

This implies that for each degree s and order t $\Lambda_{st}^{\alpha\beta\gamma\delta}$ has only 13 independent components. And for $s = 0$ and $s = 2$ this number is further reduced to 5 and 11, respectively, since $\Lambda_{st}^{\alpha\beta\gamma\delta}$ are not defined for $|\alpha+\beta+\gamma+\delta| > s$ ($\hat{Y}_s^{Nt} \equiv 0$ if $N > s$).

Based on the symmetries (30), $\delta\bar{\mathbf{m}}_{st}$ in (4) may be put into the form

$$\delta\bar{\mathbf{m}}_{st} = (q_{st}^{(1)}, q_{st}^{(2)}, \ldots, q_{st}^{(n)}) \tag{31}$$

where $n = 13$ for $s \geq 4$, and $n = (11, 5)$ for $s = (2, 0)$; the independent parameters $\{q_{st}^{(i)}, i = 1, 2, \ldots, n\}$ are defined by

$$q_{st}^{(i)} = w_i \Lambda_{st}^{\alpha_i\beta_i\gamma_i\delta_i}(r)/C(r) \tag{32}$$

with w_i being weighting coefficients and $C = \kappa(r) + \frac{4}{3}\mu(r)$ being evaluated in the reference model. We may choose the weighting coefficients w_i in such a way that the parameter set $\{q_{st}^{(i)}, i = 1, 2, \ldots, n\}$ are normalized, i.e.,

$$\sum_{s,t}\sum_{i=1}^{n}(q_{st}^{(i)})^2 \propto \int \| \Lambda \|^2 \sin\theta d\theta d\phi \qquad (33)$$

In Table 1 we tabulate the weighting coefficients together with the tensor indices α_i, β_i, γ_i, δ_i for all values of i. The differential kernel $\mathbf{M}_s$ (see (4)) corresponding to the specification $\delta\mathbf{m}_{st}$, defined in (10) and (31), then takes the form of

$$\bar{\mathbf{M}}_s = (R_s, Q_s^{(1)}, Q_s^{(2)}, \ldots, Q_s^{(13)}) \qquad (34)$$

where R_s are given in (9) and components $Q_s^{(i)}$ are obtainable from (4), (29), and (32)

$$Q_s^{(i)} = w_i \frac{r^2 C}{2\omega_0^2} g_s^{\alpha_i\beta_i\gamma_i\delta_i} \qquad (35)$$

Note that by virtue the selection rules for the 3-j symbols used in (21) $Q_s^{(i)}$ vanishes (see (23)) for $s = (0,2)$ if $i > (5,11)$.

Kernel coefficients for undulations of discontinuities. If we choose normalized undulation (divided by the radius r of the discontinuity) as the parameter δh^d in (4), the corresponding kernel coefficients can be obtained from equations (97) and (110) of *Woodhouse and Dahlen* [1978]:

$$\begin{aligned}\omega_0 H_s &= r^3[\rho(\alpha^2 - \frac{4}{3}\beta^2)\tilde{K}_s + \rho\beta^2\tilde{M}_s + \rho R_s^{(2)}]_-^+ \\ &= r^3[\kappa\tilde{K}_s + \mu\tilde{M}_s + \rho R_s^{(2)}]_-^+ \end{aligned} \qquad (36)$$

where the notation $[\cdot]_-^+$ denotes the jump discontinuity of the enclosed quantity across the boundary; and kernel $\tilde{K}_s$, $\tilde{M}_s$, and $R_s^{(2)}$ are given in equations (101),(103), and (110) of *Woodhouse and Dahlen* [1978], respectively.

TABLE 1. Weighting Coefficients w_i

	w_i	α_i	β_i	γ_i	δ_i
$i = 1$	$\sqrt{1}$	0	0	0	0
$i = 2$	$\sqrt{4}$	0	0	+	−
$i = 3$	$\sqrt{8}$	0	+	0	−
$i = 4$	$\sqrt{2}$	+	+	−	−
$i = 5$	$\sqrt{4}$	+	−	+	−
$i = 6$	$\sqrt{8}$	0	0	0	+
$i = 7$	$\sqrt{16}$	0	+	+	−
$i = 8$	$\sqrt{8}$	0	−	+	+
$i = 9$	$\sqrt{4}$	0	0	+	+
$i = 10$	$\sqrt{8}$	0	+	0	+
$i = 11$	$\sqrt{8}$	+	+	+	−
$i = 12$	$\sqrt{8}$	0	+	+	+
$i = 13$	$\sqrt{2}$	+	+	+	+

3. DATA

The theory and technique for retrieving the splitting functions of normal modes from long-period seismograms are fully described in paper 1. In paper 1 splitting function coefficients of degrees $s = 0, 2, 4$ were retrieved, for 27 multiplets, using accelerograms from the International Deployment of Accelerometers (IDA) network. For the present study we have performed the same analysis for seven additional modes, using the same data set as was used in paper 1. The results for the splitting coefficients of these seven new modes are tabulated in Table 2, which also gives estimates of the associated standard errors and the corresponding diagonal elements of the resolution matrix.

The data on which the study in paper 1 was based also constitute the data for the current study, and we do not repeat here the description of the data selection and processing. Two examples of spectral segments are shown in Figure 1. In this study we shall study the Earth structure based on the information contained in the spectral splitting of 33 modes out of 34 mentioned above. Mode ${}_{10}S_2$ is excluded from this study for the following reason. As we pointed out in paper 1, the differential kernels for mode ${}_{10}S_2$ depend strongly on the reference model we choose, due to its potential coupling with ${}_{11}S_2$. We omit it here, in order to avoid special treatment for this mode. We believe that the results and the conclusions of this study would still hold if ${}_{10}S_2$ were included, since its behavior is very similar to other *PKIKP* modes (see paper 1). The spherical harmonic coefficients of the splitting functions of the 33 multiplets, for degrees $s = 0, 2, 4$, are listed in Table 3.

4. MODELING CONCIDERATIONS AND PARAMETERIZATION

The splitting of free oscillations depends, simultaneously, on the three-dimensional distributions of P velocity, S velocity, density, boundary undulations, and anisotropy of the whole Earth. To invert for these parameters would require a much larger data set than is now available. However, the current data set can be used, together with some other assumptions and information, to retrieve certain major characters of the three-dimensional structure of the Earth. Some of the assumptions and information are based on physical considerations; e.g., the fluid outer core is assumed to be homogeneous [*Stevenson*, 1987]; some are a priori ones; for example, we will impose the constraint that heterogeneities in P velocity and in S velocity are proportional to one other; and some are experimental or even subjective assumptions; for example, we truncate the Legendre polynomial expansion in radius at certain degree. With the assistance of these assumptions and information, we seek to construct Earth models which are relatively simple, i.e., involving only a small number of modeling parameters. Of course, the model must be sufficient to adequately explain the data.

4.1. *Volumetric Perturbations in the Mantle*

Since the multiplets used in this study have very long periods (the shortest period is 193 s for mode ${}_{13}S_3$), they are sensitive only to the very large scale features of Earth structure. The distinction between the Earth's crust from the mantle, therefore, can be neglected. We simply treat the whole volume from the surface of the Earth (the seafloor for PREM model) to the core-mantle boundary as the mantle.

Although there is no evidence that lateral heterogeneity is continuous across the 670-km discontinuity, we model the heterogeneity continuously owing to the resolution of the data. Introducing a discontinuity in heterogeneity and parameterizing the upper mantle and the lower mantle separately is quite straightforward. However, we would not expect this to allow us to retrieve more information because the trade-off between the heterogeneities just above and just below the boundary is severe for the current data set. Therefore we choose to avoid this complication and to model the whole mantle continuously.

We impose the constraint that the relative aspherical perturbations in mantle P velocity (α), S velocity (β), and den-

TABLE 2. Newly Processed Splitting Functions With Their Error and Resolution Estimators

Mode	A_0^0	A_2^0	A_2^1	B_2^1	A_2^2	B_2^2	A_4^0	A_4^1	B_4^1	A_4^2	B_4^2	A_4^3	B_4^3	A_4^4	B_4^4	$\mathrm{Im}(A_0^0)$
${}_0S_4$	-479	727	-148	102	-321	-616	-101	-16	-1	85	32	-75	-43	-13	-68	-110
	27	41	48	52	63	67	39	45	43	44	43	37	41	29	27	24
	1.00	0.89	0.85	0.81	0.67	0.56	0.73	0.60	0.53	0.39	0.43	0.20	0.32	0.12	0.10	1.00
${}_0S_5$	-530	727	-289	170	-584	-760	-51	20	-61	14	-28	-74	45	92	153	-72
	21	28	23	30	38	37	26	27	29	33	32	34	32	34	32	19
	1.00	0.87	0.92	0.85	0.67	0.75	0.81	0.81	0.72	0.61	0.68	0.56	0.67	0.40	0.37	1.00
${}_0S_9$	-826	-28	-426	-131	-557	-788	55	-99	125	217	-36	-324	238	216	191	7
	19	33	23	30	34	49	29	30	35	30	31	33	34	41	38	9
	1.00	0.94	0.97	0.96	0.94	0.85	0.93	0.93	0.90	0.93	0.91	0.91	0.91	0.84	0.88	1.00
${}_2S_6$	346	-34	-528	293	374	-1050	399	129	-49	111	301	-141	154	-54	272	-52
	43	66	57	65	70	76	58	58	58	59	58	62	61	60	62	31
	1.00	0.74	0.85	0.79	0.70	0.61	0.63	0.64	0.61	0.60	0.61	0.59	0.50	0.41	0.46	1.00
${}_4S_4$	-147	331	75	53	166	-81	-199	-99	17	118	-6	61	72	-173	-66	-73
	37	36	37	36	34	29	27	24	28	23	25	21	24	26	18	35
	1.00	0.36	0.43	0.52	0.27	0.19	0.30	0.20	0.41	0.17	0.23	0.13	0.18	0.26	0.13	1.00
${}_9S_3$	336	169	121	91	-93	98	-215	-13	-18	-46	1	19	15	-167	47	7
	34	35	31	37	35	32	25	19	20	15	15	14	15	27	21	33
	1.00	0.46	0.21	0.38	0.29	0.32	0.35	0.13	0.15	0.08	0.09	0.07	0.08	0.31	0.15	1.00
${}_6S_{10}$	83	63	-24	234	-236	-600	-175	-155	-70	107	249	53	175	-66	7	-10
	27	43	34	27	43	41	34	33	31	32	32	32	33	33	32	18
	1.00	0.67	0.81	0.90	0.55	0.59	0.48	0.54	0.65	0.56	0.51	0.39	0.46	0.36	0.33	1.00

In order to comply with the convention used in expansions of the potential field (see, for example, *Stacey* [1977]), we express the splitting function (see equation (11) of *Giardini et al.* [1988]) as $\eta(\theta,\phi) = \sum_s \sum_{t=0}^{s} (A_s^t \cos t\phi + B_s^t \sin t\phi)\, p_s^t(\theta)$. The coefficients A_s^t and B_s^t are listed in unit of 10^{-6}. In the last column, imaginary parts of A_0^0 are listed, which describe the spherically symmetric corrections to the attenuation. The complex coefficients c_{st} (see (2)) can be derived from A_s^t and B_s^t as $c_{st} = (-1)^t (2\pi)^{\frac{1}{2}} (A_s^t - iB_s^t)$, for $t > 0$; $c_{st} = (4\pi)^{\frac{1}{2}} A_s^t$, for $t = 0$; and $c_{st} = (2\pi)^{\frac{1}{2}} (A_s^{|t|} + iB_s^{|t|})$, for $t < 0$. The contribution from the Earth's ellipticity of figure (see the first term in (4)) has been subtracted from the results. An estimate of the associated standard errors for the coefficients A_s^t and B_s^t is derived from the covariance matrix, and is given in the second entry for each mode (in the same unit). The third entry for each mode gives the corresponding diagonal elements of the resolution matrix.

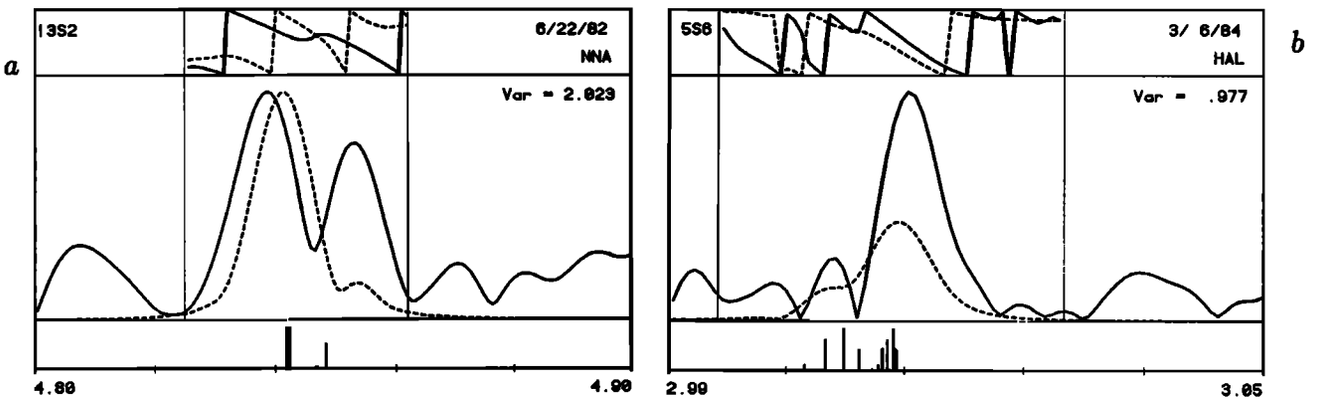

Fig. 1. Examples of data (solid curves) and synthetic spectra (dashed curves) in spectral windows. For each window the name of the multiplet, the range of the horizontal frequency axis (in millihertz), the earthquake date, and the recording station are indicated. The complex spectra are represented in terms of phase in the interval $(-\pi, \pi)$ (top panel of each figure), and amplitude on an arbitrary scale (middle panel). Vertical bars in the bottom panels indicate the frequencies and relative amplitudes of the singlets contributing to the theoretical spectra, computed for the reference model PREM, incorporating the effects of rotation and ellipticity. Vertical dotted lines delineate the portion of the signal used in the inversion. The variance ratio is a measure of the misfit between the observed and synthetic traces, computed in terms of the complex spectra. The durations and starting times (relative to event origin time) of each record are (*a*) 48, 6, (*b*) 80, 1.4, respectively, all in hours. Misfits are used to infer the aspherical structure of the Earth.

sity (ρ) are proportional to one another. The modal data used in this study are sensitive to the value of $d\ln\alpha/d\ln\beta$. Forward modeling experiments for the splitting functions of some mantle modes involved in this study indicate that the value of $d\ln\alpha/d\ln\beta$ in the lower mantle lies in the interval (0.30, 0.61) with 75% confidence (X.-D. Li, D. Giardini, and J. H. Woodhouse, submitted manuscript, 1990). This implies that a value significantly outside this interval would make it impossible to fit all the data. If we assume that the perturbations in bulk modulus and in shear modulus are positively correlated, the 75% confidence interval can be more tightly constrained to (0.39, 0.60). Clearly, there is still a relative large uncertainty in determining this value. The effect of such uncertainty on the recovery of mantle structure is not easily characterized, especially for the upper mantle where both heterogeneity and differential kernels

TABLE 3. Spherical Harmonic Coefficients of Splitting Functions

Mode	A_0^0	A_2^0	A_2^1	B_2^1	A_2^2	B_2^2	A_4^0	A_4^1	B_4^1	A_4^2	B_4^2	A_4^3	B_4^3	A_4^4	B_4^4	$\mathrm{Im}(A_0^0)$
${}_0S_3^*$	-213	226	-10	-66	18	11	13	4	-7	-7	-9	0	1	0	2	-60
${}_0S_4^*$	-479	727	-148	102	-321	-616	-101	-16	-1	85	32	-75	-43	-13	-68	-110
${}_0S_5^*$	-530	727	-289	170	-584	-760	-51	20	-61	14	-28	-74	45	92	153	-72
${}_1S_3^*$	99	14	-17	18	-1	-16	6	-7	-7	-2	0	0	0	-2	0	-248
${}_3S_1^*$	413	69	0	-12	27	-244										12
${}_0S_6^*$	-682	578	-190	5	-816	-932	34	-57	95	225	-214	-209	85	227	56	-78
${}_3S_2$	-875	1455	-31	975	169	456	-1064	399	510	-190	-100	182	-128	161	-185	139
${}_1S_4^*$	-134	33	-103	110	-160	-110	-36	48	-58	41	9	21	4	-2	8	-134
${}_0S_7^*$	-601	465	-344	117	-762	-844	7	30	41	198	-224	-325	74	45	165	-111
${}_2S_3$	609	1511	-104	207	-685	-421	173	-105	-117	-83	-3	-30	26	-61	86	37
${}_1S_5^*$	-163	283	-74	468	-597	-467	0	-70	-164	222	63	-165	-60	-46	16	-265
${}_2S_4^*$	304	236	-96	124	-855	-646	-220	-112	222	87	-84	151	-121	-238	60	-22
${}_2S_5^*$	468	404	78	109	58	-389	4	-82	-84	-158	-206	119	-34	-10	-58	-334
${}_1S_6^*$	20	315	-171	442	-742	-343	35	0	-129	31	-13	25	87	63	-5	-127
${}_0S_9^*$	-826	-28	-426	-131	-557	-788	55	-99	125	217	-36	-324	238	216	191	7
${}_1S_7^*$	-642	670	-94	166	-880	-598	-75	-75	54	192	-116	-101	178	-80	181	-189
${}_2S_6^*$	346	-34	-528	293	374	-1050	399	129	-49	111	301	-141	154	-54	272	-52
${}_1S_8^*$	-840	745	-19	202	-977	-632	0	-120	81	278	-39	-16	42	40	185	-112
${}_4S_3^*$	-288	79	46	287	-177	-372	93	60	-54	-56	-14	-141	-37	196	-127	22
${}_2S_8^*$	587	130	-325	33	2	-943	26	332	-166	-375	422	-31	240	-308	412	27
${}_5S_3^*$	-144	248	44	19	-77	-280	34	-34	-141	-41	-16	34	18	102	42	-248
${}_4S_4^*$	-147	331	75	53	166	-81	-199	-99	17	118	-6	61	72	-173	-66	-73
${}_5S_4^*$	-129	-196	-58	60	-147	-728	96	-123	-301	-28	129	-60	-134	132	-23	-81
${}_5S_5$	130	-22	-138	230	-195	-495	-88	-205	83	90	31	103	-21	-88	103	-105
${}_3S_8^*$	-41	647	-188	251	-384	-451	-16	281	63	24	115	-65	170	-53	78	-233
${}_6S_3$	37	1111	-156	495	-43	-284	383	-33	-270	323	-394	517	-62	-63	-149	-132
${}_5S_6^*$	301	81	-30	216	-265	-482	-21	-190	-54	-104	31	66	10	-21	25	-171
${}_9S_3$	336	169	121	91	-93	98	-215	-13	-18	-46	1	19	15	-167	47	7
${}_6S_{10}^*$	83	63	-24	234	-236	-600	-175	-155	-70	107	249	53	175	-66	7	-10
${}_{11}S_4$	-273	695	-31	204	-115	-56	149	-219	-123	442	-692	63	-175	-39	32	-24
${}_{13}S_2$	-98	965	-87	90	-116	-150	529	6	135	-69	296	-71	135	182	44	-39
${}_{11}S_5$	-154	711	273	209	141	-33	113	-4	-361	-199	518	238	-807	-334	-11	31
${}_{13}S_3$	30	863	-29	126	-55	-236	-4	-18	-167	-65	-175	25	-9	186	61	2

Summary of splitting function coefficients of 33 multiplets from Table 4 of *Giardini et al.* [1988] and Table 2. Modes sensitive principally to structure in the mantle are indicated by an asterisk.

are very complicated. For the lower mantle, however, the uncertainty of the value $d\ln\alpha/d\ln\beta$ has stronger effects on the amplitude than on the pattern of the inversion results. This is because the patterns of splitting functions are largely consistent between "α sensitive" modes and "β sensitive" modes. Another interesting thing to observe is that many "β sensitive" modes have high sensitivity to the topography of the core-mantle boundary (see modes ${}_0S_4$, ${}_0S_5$, ${}_0S_6$, ${}_0S_9$, ${}_3S_8$, and ${}_4S_4$ in Figure 2) while "α sensitive" modes have little sensitivity to this boundary (see modes ${}_4S_3$, ${}_5S_4$, ${}_5S_6$, and ${}_6S_{10}$ in Figure 2), implying that the amplitudes of the resulting CMB topographic models trade off with the choice of the value $d\ln\alpha/d\ln\beta$.

In this study we shall adopt a value of 0.5 for this ratio. Although we have not shown this value to be valid for the upper mantle, it is reasonable to use this value for the mantle as a whole for the following reasons: (1) some evidence has been reported that the value of $d\ln\alpha/d\ln\beta$ for the upper mantle also has a low value, possibly due to partial melting [*Hales and Doyle*, 1967]; and (2) the value which is appropriate for the lower mantle should approximate the value for the whole mantle, since the upper mantle is much less important than the lower mantle for the splitting of most modes used in this study. For the value of $d\ln\rho/d\ln\alpha$ the current modal data allow a large range of variation (X.-D. Li, D. Giardini, and J. H. Woodhouse, submitted manuscript, 1990); here we simply take the value (0.5) of *Anderson et al.* [1968] for the whole mantle. Under these assumptions we may now introduce a variable $\zeta(r,\theta,\phi)$ to describe the aspherical heterogeneities in the mantle

$$\zeta(r,\theta,\phi) = \frac{\delta\alpha(r,\theta,\phi)}{\alpha(r)} = 0.5\frac{\delta\beta(r,\theta,\phi)}{\beta(r)} = 2\frac{\delta\rho(r,\theta,\phi)}{\rho(r)} \quad (37)$$

where the denominators are evaluated in the spherical reference model.

The parameter $\zeta(r,\theta,\phi)$ may be expanded in terms of spherical harmonics in colatitude θ and longitude ϕ and in terms of normalized Legendre polynomials for the radial r dependence:

$$\begin{aligned}\zeta(r,\theta,\phi) &= \sum_{\substack{s=2\\ s\ \mathrm{even}}}^{S}\sum_{t=-s}^{s}\zeta_{st}(r)Y_s^t(\theta,\phi)\\ &= \sum_{\substack{s=2\\ s\ \mathrm{even}}}^{S}\sum_{t=-s}^{s}\sum_{k=0}^{K}\zeta_{st}^k f_k(x)Y_s^t(\theta,\phi) \quad (38)\end{aligned}$$

where S and K are the numbers at which the expansions are truncated, coefficients ζ_{st}^k are unknowns to be determined by inversion, $f_k(x)$ are Legendre polynomials as used by *Dziewonski* [1984], $Y_s^t(\theta,\phi)$ are spherical harmonics as defined by *Edmonds* [1960], and x is reduced, normalized radius running from -1 at the core-mantle boundary to $+1$ at the surface of the Earth (the seafloor).

It is not appropriate to assume a relation of the form (37) for the spherical part of the perturbation, and therefore for

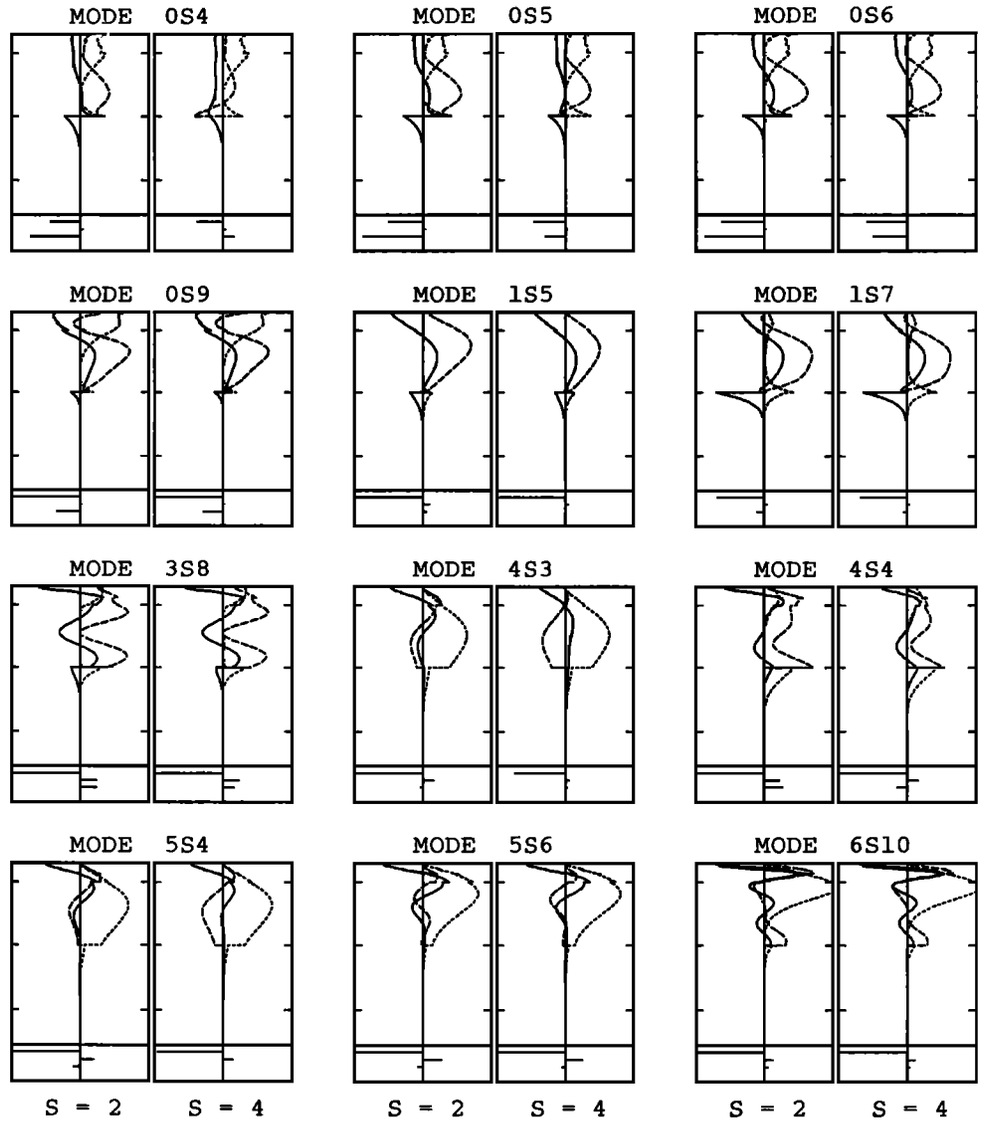

Fig. 2. Differential kernels for spherical harmonic degrees 2 and 4 of some mantle modes. The sensitivities of splitting functions, as a function of depth, to perturbations in v_P (dotted curves), v_S (dashed curves), and ρ (solid curves) are plotted in the top panels. On side margins, the 670-km discontinuity, the core-mantle boundary (CMB), and the inner core boundary (ICB) are marked from top down. The kernels are defined in (7), (8), (9). The horizontal scale is $\pm 4/a$, where a is the radius of the Earth. In each bottom panel, kernel coefficients H_s defined in (36) are plotted, from top to bottom, for the free surface, the 670-km discontinuity, the CMB, and the ICB, with ± 1 being the horizontal scale. The kernels for the ICB of these modes are so small that they vanish from sight.

degree $s = 0$ we determine independent perturbations in P and S velocities and density, writing

$$\frac{\delta\alpha_0}{\alpha} = \sum_{k=0}^{K} \alpha^{(k)} f_k(x) \tag{39}$$

$$\frac{\delta\beta_0}{\beta} = \sum_{k=0}^{K} \beta^{(k)} f_k(x) \tag{40}$$

$$\frac{\delta\rho_0}{\rho} = \sum_{k=0}^{K} \rho^{(k)} f_k(x) \tag{41}$$

where $\delta\alpha_0$, $\delta\beta_0$, and $\delta\rho_0$ are the spherical perturbations from the reference model and $\alpha^{(k)}$, $\beta^{(k)}$, and $\rho^{(k)}$ are unknown constants.

4.2. *Boundary Undulations*

The modes used in this study are very sensitive to aspherical structure at the very top part of the mantle, including undulations of the discontinuities. Figures 2 and 3 show the sensitivities of several modes to perturbations in the radius of the surface (the seafloor for the PREM model), together with the sensitivities to other features of the Earth. The strong sensitivities to the surface undulation are evident. The sensitivities to the other main discontinuity near the surface, the Moho, are not shown, but they are comparable in magnitude with those to the seafloor. Since the wavelengths of the modes used in this study are much longer than the distance between these two discontinuities, it would give misleading results if any or both of these discontinuities were inverted for from the modal data. Trade-offs between

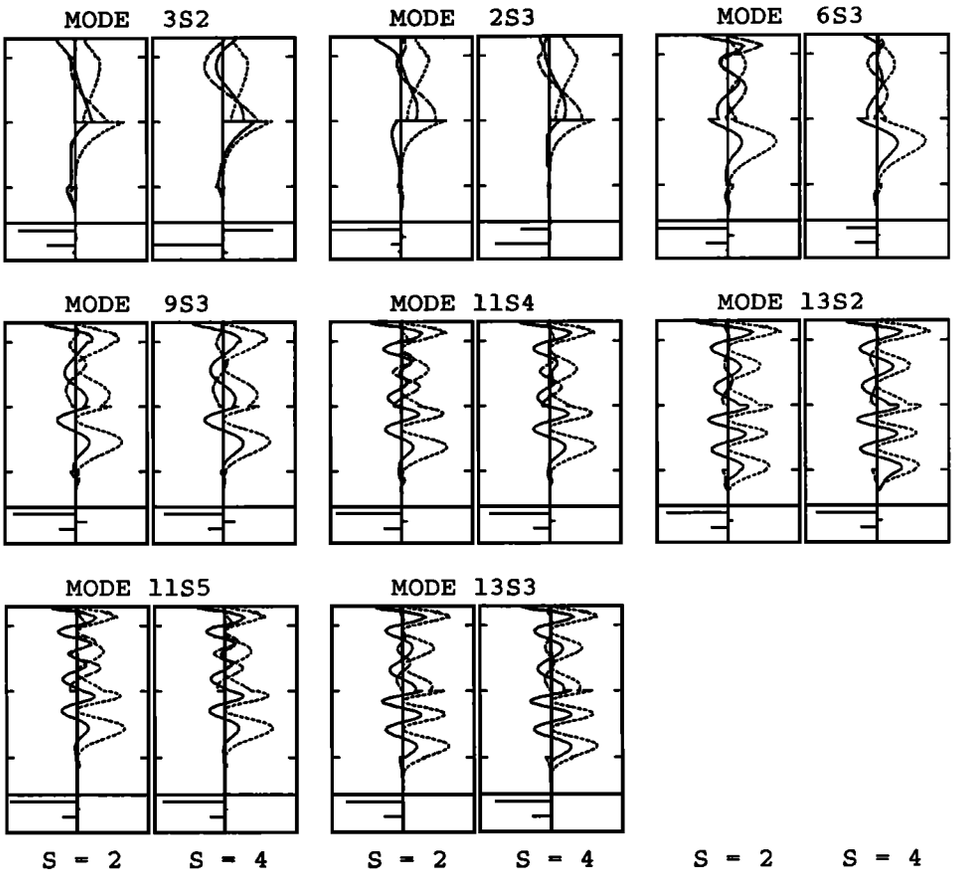

Fig. 3. Differential kernels for spherical harmonic degrees 2 and 4 of some core modes. The sensitivities of these mode penetrate deeply into the core. See caption to Figure 2 for details, with exceptions that the sensitivities to the undulation of the inner core boundary of some modes presented here are visible now.

the volumetric perturbation at the top of the mantle and the undulations of these two boundaries are also expected. Therefore we elect to ignore the perturbations of these discontinuities, and correspondingly their effects may contaminate the results of the inversion for volumetric heterogeneity at the top part of the mantle. *Ritzwoller et al.* [1988] modeled mantle structure only of spherical harmonic degree $s = 2$ by using modal data. They also found that the splitting data for mantle modes (most of the modes they used coincide with the ones used in this study) are not sufficient to infer uppermost mantle structure unambiguously, even with the assistance of the constraints provided by the frequency measurements for many fundamental surface wave equivalent modes of *Smith et al.* [1987].

The 670-km discontinuity and the inner core boundary are also not included in the inversions, owing to the poor constraints which the data set provide for these parameters. The low sensitivities to the 670-km discontinuity are clear in Figures 2 and 3, and only a small number of "core modes" are sensitive to the inner core boundary (see Figure 3).

We do include in the inversion the topography of the core-mantle boundary (CMB). Although we do not expect to obtain unequivocal results for CMB topography, because of the low resolution of the current data, we show that some characteristics of the CMB are revealed by this experiment. A number of modes used in this study are sensitive to the perturbation of the CMB and some have very strong sensitivities: for example, see the kernels for modes ${}_0S_4$, ${}_0S_5$, and ${}_0S_6$ in Figure 2 and modes ${}_3S_2$ and ${}_2S_3$ in Figure 3.

4.3. *Anisotropy in the Inner Core*

The necessity of introducing inner core anisotropy to explain the behavior of the anomalously split core modes has been argued in previous studies [*Woodhouse et al.*, 1986; *Giardini et al.*, 1987]. The splitting of eight core modes is used to constrain inner core anisotropy. It would certainly be advantageous to employ more modes. However, for the earthquakes used in this study (see Table 2 of paper 1), we have examined the spectra recorded by the IDA network and found that it is difficult to expand the data set significantly. Future large, deep events will probably yield data enabling better constraints to be placed upon inner core structure. Since we do not have sufficient data to derive a unique model, even for lower degrees, the result achieved by solving this underdetermined inverse problem should be regarded only as an example of a model which fits the data. The model we obtain may, however, reflect some realistic features, such as the magnitude of inner core anisotropy.

In the discussion here we shall omit mentioning anisotropy of degree zero; such anisotropy corresponds to transverse isotropy about the radial vector which does not contribute to splitting but acts only to shift the central frequency of the mode. Although there are components of degree zero in the anisotropic models to be presented, the corresponding pa-

rameters will trade off with all other spherically symmetric perturbations and thus are not well determined. Since the splitting functions of the anomalously split modes are dominated by coefficients c_{20} and c_{40} [*Woodhouse et al.*, 1986; *Giardini et al.*, 1987; paper 1], we invert for the cylindrically symmetric part (i.e., spherical harmonic order $t = 0$) of anisotropy only. As a result of section 2.2, we need 24 (11 for $s = 2$ and 13 for $s = 4$) independent parameters to describe such an anisotropic tensor field A, which is subject to the symmetry property (30), on a sphere. Generally speaking, these parameters are functions of radius r. Assuming that inner core anisotropy varies smoothly with r and only terms associated with r^0, r^1, and r^2 remain in the expansion for the radial dependence, the total number of independent parameters which are needed to determine A would appear to number to 72. However, the requirement that the elastic tensor be nonsingular at the center of the Earth reduces the number to 14. Furthermore, we may also assume that the there are no lateral variations in chemical properties and the thermal condition in the inner core and that the zonal structure is purely due to the axisymmetric spatial distribution of the crystal orientations. This working hypothesis is by no means required by the data. However, since it represents a physically simpler model and is consistent with the current modal data (as we show below), we shall make this assumption. Thus only 12 (constant) parameters are needed to describe such an anisotropic inner core model. If anisotropy of degree zero is included in the inversion, six more parameters are introduced. Specifically, we write

$$c_{00} = \sum_{i=1}^{6} \Psi_0^{(i)} \psi_0^{(i)} \tag{42}$$

$$c_{20} = \sum_{i=1}^{7} \Psi_2^{(i)} \psi_2^{(i)} \tag{43}$$

$$c_{40} = \sum_{i=1}^{5} \Psi_4^{(i)} \psi_4^{(i)} \tag{44}$$

where $\psi_s^{(i)}$ are the constant parameters describing the anisotropic field and $\Psi_s^{(i)}$ are the associated kernel coefficients which are known. A recipe for choosing parameters $\psi_s^{(i)}$ and the associated coefficients $\Psi_s^{(i)}$ is given in the appendix.

4.4. *Attenuation Structure in the Mantle*

As we restrict the inversion only to the spherically symmetric components of the imaginary part of splitting function (see paper 1; also Table 2 in the present paper), we invert only for the spherically symmetric perturbation in the attenuation structure of the Earth. Although it is straightforward to include lateral variations in attenuation, it would lead to only insignificant additional variance reduction, as pointed out in paper 1.

In modeling, an assumption will be made that the imaginary part of shear modulus departs from the reference model (PREM) by $\delta\bar{\mu}(r)$, while the imaginary part of bulk modulus is fixed as in the reference model. Thus we can write

$$\omega_0 \operatorname{Im}(c_{00}) = \int_{r_C}^{r_S} \frac{\delta\bar{\mu}(r)}{\mu(r)} \mu(r) M_0(r) r^2 dr \tag{45}$$

where ω_0 is the real part of reference frequency of the multiplet, $\mu(r)$ is the shear modulus evaluated in the reference model, $M_0(r)$ is the differential kernel given by equation (102) of *Woodhouse and Dahlen* [1978], and r_S and r_C are the radii of the seafloor and the core-mantle boundary, respectively. As for $\zeta_s^t(r)$ in (38), we expand:

$$\frac{\delta\bar{\mu}(r)}{\mu(r)} = \sum_{k=0}^{K} \bar{\mu}^{(k)} f_k(x) \tag{46}$$

where $\bar{\mu}^{(k)}$ are the constants to be found and $f_k(x)$ are those defined when they are introduced in (38).

4.5. *Summary*

To summarize the discussion of this section, we here list the assumptions made in constructing Earth models:

1. Earth structure is modeled only for spherical harmonic degrees $s = 0, 2, 4$.
2. The heterogeneity in the upper mantle and that in the lower mantle are not parameterized separately, since the data do not have enough resolution to determine if the heterogeneity is continuous across the 670-km discontinuity.
3. The relationship $\delta \ln \beta = 2\delta \ln \alpha = 4\delta \ln \rho$ is imposed for the mantle.
4. With the exception of the core-mantle boundary the topography of internal boundaries is not included in the inversions.
5. A relatively simple model of inner core anisotropy is assumed. The model is required to vary smoothly throughout the inner core and to be cylindrically symmetric about the Earth's rotation axis.
6. The attenuation rates of different singlets within a multiplet is assumed to be the same. The perturbations in attenuation of multiplets are attributed to spherical perturbations in the imaginary part of shear modulus in the mantle.

5. MODELING APPROACHES

Using the c_{st} coefficients listed in Table 3 as data, an inverse problem is defined by (4) where $\delta\mathbf{m}_{st}$ and δh_{st}^d are treated as unknowns. The problem can be solved by regular linear least squares methods.

An alternative procedure is to find Earth models to fit directly the original split spectra from which we have retrieved our splitting function coefficients. The inverse problem is in principle posed by (1), (2), and (4): retrieving the Earth structure $\delta\mathbf{m}_{st}$ and δh_{st}^d from data $\mathbf{u}(t)$. This is a nonlinear problem, and we solve it iteratively.

The first procedure obviously has a great advantage. Having retrieving splitting function coefficients, c_{st}, accurately enough, the problem becomes very simple. The model parameters of spherical harmonic degree s and order t are controlled only by the splitting function coefficients of the same degree and order, as indicated by (4). Therefore the inverse problem is decoupled into a number of low-dimensional linear problems. This enables us to do many experiments to test the a priori constraints on the models. As more high-quality digital seismic stations are deployed and as these stations record more large events, we can continually retrieve new c_{st} coefficients for different modes and for higher degrees and improve those results which are not well-constrained.

Although following the second method is a time-consuming procedure, we think it is still valuable, at this stage, to solve

the problem by directly fitting the original seismic traces. When we invert for splitting functions mode by mode, there is no guarantee that the resulting splitting function is the unique solution which represents a property of the Earth. If the splitting function solution is not the one corresponding to reality, we are in danger of inferring erroneous models or of not being able to find any satisfactory model. By following the second procedure, we should overcome the possible inconsistency of the inferred splitting functions, since they are constrained by the requirement that they all be consistent with a single Earth model. Models developed by such a one-step method are also expected to be statistically better constrained.

5.1. *Formalism of Inverse Theory*

Inverse problems are encountered in two different contexts. In both cases, we seek Earth models, represented by unknown vector $\mathbf{x}$, which can explain modal data $\mathbf{d}$, which are either splitting function coefficients as tabulated in Table 3 or the original seismic spectra. Without loss of generality, the inverse problems arising in this study may be stated as follows: we seek a discrete set of parameters, represented by model vector $\mathbf{x}$, satisfying

$$\begin{cases} \mathbf{d} = \mathbf{f}(\mathbf{x}) + \mathbf{e} \\ \mathbf{B}\mathbf{x} = \mathbf{g} \end{cases} \tag{47}$$

where the first equation is the basic equation and the second one imposes an additional constraint, which could be trivial. In (47) the vector $\mathbf{d}$ is a collection of data of dimension N, the function $\mathbf{f}$ could be either linear or nonlinear; $\mathbf{x}$ has finite dimension M, vector $\mathbf{e}$ represents stochastic errors associated with $\mathbf{d}$, matrix $\mathbf{B}$ has dimension of $N' \times M$ with $0 \leq N' < M$, and $\mathbf{g}$ is a known vector of dimension N', containing additional constraints on Earth models; for example, those provided by *PKIKP* travel times. For $N' = 0$, the constraint $\mathbf{B}\mathbf{x} = \mathbf{g}$ is trivial.

One general way to solve the inverse problem (47) is to employ a stochastic formulation [*Jackson*, 1979; *Tarantola and Valette*, 1982; *Gubbins and Bloxham*, 1985]. We assume in what follows that the errors $\mathbf{e}$ are independent samples from a normal distribution having zero mean and variance σ_e^2. The data covariance matrix $\mathbf{C}_e$ therefore is the diagonal matrix having all diagonal entries equal to σ_e^2. We also assume that when the constraint $\mathbf{B}\mathbf{x} = \mathbf{g}$ is ignored, the model parameters $\mathbf{x}$ are Gaussian variables and have a priori mean value $\mathbf{x}_0$ with a certain covariance matrix $\mathbf{C}_x$. Under these assumptions, the posteriori probability distribution of model vector $\mathbf{x}$ is given by

$$\begin{aligned} P(\mathbf{x}) \propto \exp\{-\tfrac{1}{2}(\mathbf{f}(\mathbf{x}) - \mathbf{d})^T \mathbf{C}_e^{-1} (\mathbf{f}(\mathbf{x}) - \mathbf{d})\} \\ \times \exp\{-\tfrac{1}{2}(\mathbf{x} - \mathbf{x}_0)^T \mathbf{C}_x^{-1} (\mathbf{x} - \mathbf{x}_0)\} \end{aligned} \tag{48}$$

This relation indicates that the maximum likelihood solution to $\mathbf{d} = \mathbf{f}(\mathbf{x}) + \mathbf{e}$ is obtainable by minimizing the objective function

$$\Phi(\mathbf{x}) = (\mathbf{f}(\mathbf{x}) - \mathbf{d})^T \mathbf{C}_e^{-1} (\mathbf{f}(\mathbf{x}) - \mathbf{d}) + (\mathbf{x} - \mathbf{x}_0)^T \mathbf{C}_x^{-1} (\mathbf{x} - \mathbf{x}_0) \tag{49}$$

The minimum of $\Phi(\mathbf{x})$ subject to the constraint $\mathbf{B}\mathbf{x} = \mathbf{g}$ is found by the iterative application of the recursion

$$\begin{aligned} \begin{bmatrix} \mathbf{x}_{i+1} \\ \lambda \end{bmatrix} = \begin{bmatrix} \mathbf{x}_i \\ \mathbf{0} \end{bmatrix} + \begin{bmatrix} \mathbf{A}_i^T \mathbf{C}_e^{-1} \mathbf{A}_i + \mathbf{C}_x^{-1} & \mathbf{B}^T \\ \mathbf{B} & \mathbf{0} \end{bmatrix}^{-1} \\ \times \begin{bmatrix} \mathbf{A}_i^T \mathbf{C}_e^{-1} (\mathbf{d} - \mathbf{f}(\mathbf{x}_i)) - \mathbf{C}_x^{-1} (\mathbf{x}_i - \mathbf{x}_0) \\ \mathbf{g} - \mathbf{B}\mathbf{x}_i \end{bmatrix} \end{aligned} \tag{50}$$

where λ is a vector Lagrange multiplier of dimension N' and $\mathbf{A}_i$ is the $N \times M$ matrix of partial derivatives

$$\mathbf{A}_i = \left[\frac{\partial \mathbf{f}(\mathbf{x})}{\partial \mathbf{x}} \right]_{\mathbf{x}=\mathbf{x}_i} \tag{51}$$

When splitting function coefficients are used as data $\mathbf{d}$, $\mathbf{A}_i$ is just a constant matrix (with respect to i), which can be evaluated readily based on the formulation developed in section 2. For the case in which $\mathbf{d}$ represents seismic traces, $\mathbf{A}_i$ is calculated for each iteration by using the chain rule for differentiation and by using the formulation presented in paper 1 and in section 2 of this paper.

In this study the a priori model $\mathbf{x}_0$ is always taken to be zero. Namely, we are always seeking solutions which are small perturbations from a known spherical reference model. Correspondingly the model covariance matrix $\mathbf{C}_x$ quantifies the strength of our desire for smallness of the model $\mathbf{x}$. And the matrix $\mathbf{C}_x$ can always be diagonalized provided $\mathbf{x}$ is chosen to be associated with orthogonal bases. Thus (50) becomes

$$\begin{aligned} \begin{bmatrix} \mathbf{x}_{i+1} \\ \lambda \end{bmatrix} = \begin{bmatrix} \mathbf{x}_i \\ \mathbf{0} \end{bmatrix} + \begin{bmatrix} \mathbf{A}_i^T \mathbf{C}_e^{-1} \mathbf{A}_i + \varsigma \mathbf{C}_x^{-1} & \mathbf{B}^T \\ \mathbf{B} & \mathbf{0} \end{bmatrix}^{-1} \\ \times \begin{bmatrix} \mathbf{A}_i^T \mathbf{C}_e^{-1} (\mathbf{d} - \mathbf{f}(\mathbf{x}_i)) - \varsigma \mathbf{C}_x^{-1} \mathbf{x}_i \\ \mathbf{g} - \mathbf{B}\mathbf{x}_i \end{bmatrix} \end{aligned} \tag{52}$$

where ς is the parameter which quantifies the overall strength of the desire for the smallness of the model and $\mathbf{C}_x$ is now diagonalized and has diagonal entries equal to σ_i^2 ($i = 1, 2, \ldots, M$); σ_i specify the relative strength of each model parameter x_i.

Since the concept of resolution does not easily extend to nonlinear problems, we analyze resolution only for the linearized problem in the neighborhood of the model, $\mathbf{x}_\infty$, to which (52) converges.

Let us suppose that we have obtained a solution $\mathbf{x}_i$ in the neighborhood of $\mathbf{x}_\infty$. We may introduce a variation of the model, $\delta\mathbf{x}$, which would cause the variations of data $\mathbf{d}$ and $\mathbf{g}$ by $\delta\mathbf{d} = \mathbf{A}\delta\mathbf{x}$ and $\delta\mathbf{g} = \mathbf{B}\delta\mathbf{x}$ with $\mathbf{A} \equiv \mathbf{A}_\infty$. Thus the variation of our solution $\mathbf{x}_{i+1}$ is, according to (52), given by

$$\delta\mathbf{x}_{i+1} = (\mathbf{G}^{(1)} \mathbf{A}^T \mathbf{C}_e^{-1} \mathbf{A} + \mathbf{G}^{(2)} \mathbf{B}) \delta\mathbf{x} \tag{53}$$

where the $M \times M$ matrix $\mathbf{G}^{(1)}$ and the $M \times N'$ matrix $\mathbf{G}^{(2)}$ are submatrices defined through

$$\begin{bmatrix} \mathbf{G}^{(1)} & \mathbf{G}^{(2)} \\ \mathbf{G}^{(3)} & \mathbf{G}^{(4)} \end{bmatrix} = \begin{bmatrix} \mathbf{A}_i^T \mathbf{C}_e^{-1} \mathbf{A}_i + \varsigma \mathbf{C}_x^{-1} & \mathbf{B}^T \\ \mathbf{B} & \mathbf{0} \end{bmatrix}^{-1} \tag{54}$$

where $\mathbf{G}^{(3)}$ and $\mathbf{G}^{(4)}$ are, of necessity, $N' \times M$ and $N' \times N'$ matrices, respectively. The resolution matrix $\mathbf{R}$ of our inversion may, therefore, be defined by virtue of (53):

$$\mathbf{R} \equiv \mathbf{G}^{(1)} \mathbf{A}^T \mathbf{C}_e^{-1} \mathbf{A} + \mathbf{G}^{(2)} \mathbf{B} \tag{55}$$

The resolution parameter $R = \operatorname{tr} \mathbf{R} - N'$ represents the effective number of degrees of freedom of the solution [*Gubbins and Bloxham*, 1985].

Similarly, the linearized analysis yields the covariance matrix of the model sampling distribution which, according to (52), is given by

$$\mathbf{C} \equiv \langle \left[\frac{\partial \mathbf{x}_{i+1}}{\partial \mathbf{d}}\mathbf{e}\right] \cdot \left[\frac{\partial \mathbf{x}_{i+1}}{\partial \mathbf{d}}\mathbf{e}\right]^T \rangle = \mathbf{G}^{(1)}\mathbf{A}^T\mathbf{C}_e^{-1}\mathbf{A}\mathbf{G}^{(1)} \quad (56)$$

where angle brackets denotes the expectation of the enclosed quantity and we have used the fact that $\langle \mathbf{e} \cdot \mathbf{e}^T \rangle = \mathbf{C}_e$ and that $\mathbf{G}^{(1)}$ is a symmetric matrix.

In order to evaluate the matrix $\mathbf{C}$, the diagonal entries σ_e^2 of the data covariance matix $\mathbf{C}_e$ may be estimated a posteriori from the formula

$$\sigma_e^2 = \frac{(\mathbf{d} - \mathbf{f}(\mathbf{x}))^T(\mathbf{d} - \mathbf{f}(\mathbf{x}))}{N - R} \quad (57)$$

The standard error associated with model parameter x_i then will be $[C_{ii}]^{\frac{1}{2}}$.

Note that the posteriori model covariance matrix $\mathbf{C}$ and the resolution matrix $\mathbf{R}$, and thus the error and resolution estimates, are calculated for the given a priori information ς and σ_i. The dependence of the results on such information, especially on ς, can be very strong for underdetermined inverse problems. In such a case, the error and resolution estimates become very conditional. The lack of a priori information, corresponding to imposing small ς, can lead to a large uncertainty in the solution. On the other hand, imposing strong a priori constraints (i.e., choosing ς too large) will result in error estimates unrealistically small.

5.2. *Modeling Splitting Functions*

Using the splitting function coefficients listed in Table 3 as data, we have inverted for Earth models by linear least squares methods. Here we describe two aspherical Earth models which are retrieved from the aspherical part ($s = 2$ and $s = 4$) of the splitting function coefficients listed in Table 3. The first is a heterogeneous model of the mantle and the second is an anisotropic model of the inner core.

Although the splitting function coefficients of degree 0 (A_0^0 and $\mathrm{Im}(A_0^0)$ in Table 3) provide high-quality constraints on spherical Earth models (see paper 1), the quantity of these coefficients is not sufficient to improve upon spherical models. Our reference spherical model (PREM of *Dziewonski and Anderson* [1981]) is based on a much larger data set than that used in this study. We expect that the spherical corrections to PREM will be characterized by high degrees in the radial expansion, which are not well constrained by our data. For these reasons we choose not to model the coefficients A_0^0 and $\mathrm{Im}(A_0^0)$ at this stage.

Aspherical model of mantle. For the current experiment we use the c_{st} coefficients of 25 mantle modes (those indicated by an asterisk in Table 3) as vector $\mathbf{d}$ and truncate the expansion of $\zeta_{st}(r)$ at $K = 6$ in (38) to model the volumetric perturbation in the mantle. We invert for the topography of the CMB simultaneously. Thus the elements of unknown vector $\mathbf{x}$ are ζ_{st}^0, ζ_{st}^1, ..., ζ_{st}^6, and δh_{st} (the relative perturbation in the radius of the CMB),eight unknowns for each s and t.

In order to approximate the assumption that the elements in the vector $\mathbf{e}$ (as defined in (47)) are independent samples from a normal distribution, we should divide each splitting function coefficients, c_{st}, by its associated error when it is used as an element of vector $\mathbf{d}$ in (47). Naturally one would consider using the error estimates listed in Table 4 of paper 1 and Table 2 to evaluate the error $\mathbf{e}$; however, we find that the error estimates for modes which have very small splitting effect (e.g., ${}_1S_3$) are usually unrealistically small, compared with those of the other modes, due to the damping used in the inversion for the splitting functions. This bias in the error estimates of the splitting functions forces us to select another option: we simply assume that all splitting function coefficients have the same standard errors and we let them enter into vector $\mathbf{d}$ with the same weight.

Now we turn our attention to the specification of the elements, σ_i^2, of the model covariance matrix $\mathbf{C}_x$ (see (52)). The orthonormality of Legendre polynomials enables us put $\sigma_i = \sigma_\zeta$ for all i corresponding to ζ_{st}^k, $k = 0, 1, \ldots, 6$. Since we can incorporate any common factor multiplying the elements σ_i into parameter ς (see (52)), the remaining problem in evaluating σ_i is to choose the ratio of the element σ_h, corresponding to δh_{st}, to the other diagonal elements σ_ζ, corresponding to ζ_{st}^k ($k = 0, 1, \ldots 6$). To seek a priori information on this issue, we have compared the size of a lower mantle P velocity model (V.3 of *Morelli and Dziewonski* [1987*b*]) and the size of a CMB topography model [*Morelli and Dziewonski*, 1987*a*]. (The comparison has been made only for harmonic degree $s = 2$ and $s = 4$). The result corresponds to $\mathrm{rms}(\zeta_{st}^k)/\mathrm{rms}(\delta h_{st}) = 0.5$ for our case (actually we are interested only in the order of magnitude of this value, if the inverse problem is a stable one). This suggests that we set $\sigma_\zeta/\sigma_h = 0.5$ to specify the strengths of desire for the relative smallness to volumetric and boundary perturbations.

The damping parameter ς determines the general strength of the desire for smallness of the model relative to the fit to the data. It is a trade-off parameter and is chosen so that the variance in data is reduced close to its minimum while the size of the model is kept reasonably small. This needs a subjective judgement.

The model we thus obtained is named SAF (Splitting data, Aspherical model, from splitting Functions), and it is tabulated in Table 4. Along with the coefficients of the model, we also list in Table 4 the estimates of the associated standard errors and the corresponding diagonal elements of the resolution matrix. The standard errors are derived from the covariance matrix of the model sampling distribution (see (56)). The obvious tendency is that the resolution becomes poorer for coefficients of higher degree in the radial expansion. This is expected, and implies that although we could introduce higher degrees than $k = 6$ in the inversion, they would not be well be resolved by the data. Therefore the truncation of the expansion of $\zeta_{st}(r)$ in (38) is justified.

In Table 5 the misfit to each mode of this model is listed. The total variance reduction is as high as 77%. However, the rms of the residuals in the data is larger by a factor of 3.3 than that of the error estimates listed in Table 4 of paper 1 and Table 2 of this paper. (The error estimates listed in Table 4 of paper 1 need to be divided by $\sqrt{2}$ to correct a mistake in calculation.) If we believe that these error estimates are underestimated by a factor of $\sqrt{2}$ due to ignoring the windowing effect(J. Park, personal communication, 1987; also see paper 1), the residuals are still above the error level by a factor 2.3. One might argue that model SAF does not fit the splitting functions. But we rather explain it as the underestimation of the errors associated with the splitting functions, due to the damping in the inversions and

TABLE 4. Model SAF

	${}^kA_2^0$	${}^kA_2^1$	${}^kB_2^1$	${}^kA_2^2$	${}^kB_2^2$	${}^kA_4^0$	${}^kA_4^1$	${}^kB_4^1$	${}^kA_4^2$	${}^kB_4^2$	${}^kA_4^3$	${}^kB_4^3$	${}^kA_4^4$	${}^kB_4^4$
$k=0$	156	-67	66	-172	-250	-4	10	0	36	18	-32	54	-19	58
	15	15	15	15	15	19	19	19	19	19	19	19	19	19
	0.92	0.92	0.92	0.92	0.92	0.91	0.91	0.91	0.91	0.91	0.91	0.91	0.91	0.91
$k=1$	-157	-69	-13	197	-72	47	43	-49	-57	85	-44	42	-1	62
	28	28	28	28	28	33	33	33	33	33	33	33	33	33
	0.58	0.58	0.58	0.58	0.58	0.66	0.66	0.66	0.66	0.66	0.66	0.66	0.66	0.66
$k=2$	59	-14	-53	110	-36	-2	73	36	-53	37	27	22	-57	14
	28	28	28	28	28	34	34	34	34	34	34	34	34	34
	0.54	0.54	0.54	0.54	0.54	0.57	0.57	0.57	0.57	0.57	0.57	0.57	0.57	0.57
$k=3$	48	-55	-29	-106	-58	27	29	52	20	-67	-54	10	20	48
	28	28	28	28	28	38	38	38	38	38	38	38	38	38
	0.34	0.34	0.34	0.34	0.34	0.45	0.45	0.45	0.45	0.45	0.45	0.45	0.45	0.45
$k=4$	-34	-8	-50	3	83	-3	-15	7	47	-39	-51	22	49	-18
	22	22	22	22	22	30	30	30	30	30	30	30	30	30
	0.25	0.25	0.25	0.25	0.25	0.29	0.29	0.29	0.29	0.29	0.29	0.29	0.29	0.29
$k=5$	7	-9	4	-19	59	15	41	23	21	-13	-26	6	28	-4
	21	21	21	21	21	27	27	27	27	27	27	27	27	27
	0.15	0.15	0.15	0.15	0.15	0.15	0.15	0.15	0.15	0.15	0.15	0.15	0.15	0.15
$k=6$	13	-14	7	2	-12	33	25	2	-25	-16	-9	-23	3	20
	17	17	17	17	17	24	24	24	24	24	24	24	24	24
	0.08	0.08	0.08	0.08	0.08	0.11	0.11	0.11	0.11	0.11	0.11	0.11	0.11	0.11
$k=c$	-101	115	40	84	319	-24	35	5	-8	44	82	-1	-80	-71
	54	54	54	54	54	70	70	70	70	70	70	70	70	70
	0.67	0.67	0.67	0.67	0.67	0.54	0.54	0.54	0.54	0.54	0.54	0.54	0.54	0.54

Parameter $\zeta(r,\theta,\phi)$ in (37) is expressed (see the legend to Table 2) as $\zeta(r,\theta,\phi) = \sum_s \sum_{t=0}^{s} \sum_{k=0}^{K} ({}^kA_s^t \cos t\phi + {}^kB_s^t \sin t\phi) f_k(x) p_s^t(\theta)$; and the relative perturbation in CMB radius δh is expressed in same convention $\delta h = \sum_s \sum_{t=0}^{s} ({}^cA_s^t \cos t\phi + {}^cB_s^t \sin t\phi) p_s^t(\theta)$, where $f_k(x)$ are Legendre polynomials and $p_s^t(\theta)$ are spherical harmonics. The complex coefficients ζ_{st}^k in (38) can be derived from ${}^kA_s^t$ and ${}^kB_s^t$ as $\zeta_{st}^k = (-1)^t(2\pi)^{\frac{1}{2}}({}^kA_s^t - i\,{}^kB_s^t)$, for $t > 0$; $\zeta_{st}^k = (4\pi)^{\frac{1}{2}}\,{}^kA_s^t$, for $t = 0$; and $\zeta_{st}^k = (2\pi)^{\frac{1}{2}}({}^kA_s^{|t|} + i\,{}^kB_s^{|t|})$, for $t < 0$. The coefficients ${}^kA_s^t$ and ${}^kB_s^t$ are given in the first entry for each degree k in unit of 10^{-6}. An estimate of the associated error for the coefficients ${}^kA_s^t$ and ${}^kB_s^t$ is derived from the covariance matrix, and is given in the second entry (in the same unit). The third entry for each degree k gives the corresponding diagonal elements of the resolution matrix.

TABLE 5. Misfit to Each Mode of Model SAF

Mode	Normalized χ^2 Misfit
${}_0S_3$	0.20
${}_0S_4$	0.19
${}_0S_5$	0.10
${}_1S_3$	0.26
${}_3S_1$	0.09
${}_0S_6$	0.17
${}_1S_4$	0.19
${}_0S_7$	0.12
${}_1S_5$	0.16
${}_2S_4$	0.47
${}_2S_5$	0.36
${}_1S_6$	0.16
${}_0S_9$	0.43
${}_1S_7$	0.15
${}_2S_6$	0.67
${}_1S_8$	0.16
${}_4S_3$	0.16
${}_2S_8$	0.28
${}_5S_3$	0.09
${}_4S_4$	0.35
${}_5S_4$	0.43
${}_5S_5$	0.17
${}_3S_8$	0.18
${}_5S_6$	0.09
${}_6S_{10}$	0.19
average	0.23

The misfit is defined by $\chi^2 = \frac{1}{\sigma^2}[\sum_{i=1}^{N_j}(c_i - c_i^P)^2/N_j]$, where N_j is the number of coefficients used in inversion of mode j, c_i are the observed splitting function coefficients, c_i^P are the predicated splitting function coefficients from model SAF, and $\sigma^2 \equiv \sum_{i=1}^{N} c_i^2/N$, with $N = \sum_j N_j$.

due to the violation of some assumptions which are made in retrieving the splitting functions

Modeling inner core anisotropy. The splitting functions of anomalously split modes cannot be explained by mantle structure alone. Taking c_{20} and c_{40} of 8 core modes (whose differential kernels are plotted in Figure 3) as data, the variance reduction by model SAF is only 29%. Here we shall attempt to model the residual splitting functions of these modes by inner core anisotropy which is assumed to take the form as described in the appendix. Namely, we solve (47) for the unknown vector $\mathbf{x}$ which contains $\{\psi_2^{(i)}, i = 1,2,\ldots,7\}$ for $s = 2$ and $\{\psi_4^{(i)}, i = 1,2,\ldots,5\}$ for $s = 4$. Again, as we did during inverting for model SAF, we let splitting function coefficients enter into vector $\mathbf{d}$ with the same weight. Since the parameter set $\{\psi_s^{(i)}\}$ is associated with a set of orthonormal basis tensors, all the elements of the a priori model covariance matrix $\mathbf{C}_x$ are set to ς^{-1}.

For a given damping level, ς, we may solve the least squares problem and check the size of the resulting model and the fit to the data (residual splitting function coefficients). We also calculate the synthetic *PKIKP* travel times from the resulting anisotropic model. In Figure 4 we plot the predicted travel times of the rays which vertically penetrate the inner core, along with the associated error estimates, against the value of $\log 1/\varsigma$.

For $s = 2$, the model can essentially predict the travel times reported by *Morelli et al.* [1986] and by *Shearer et al.* [1988] for values of $\log 1/\varsigma$ greater than 6.9. For $s = 4$ the observed travel times place stricter requirements on the value of ς (or equivalently on the size of the model)

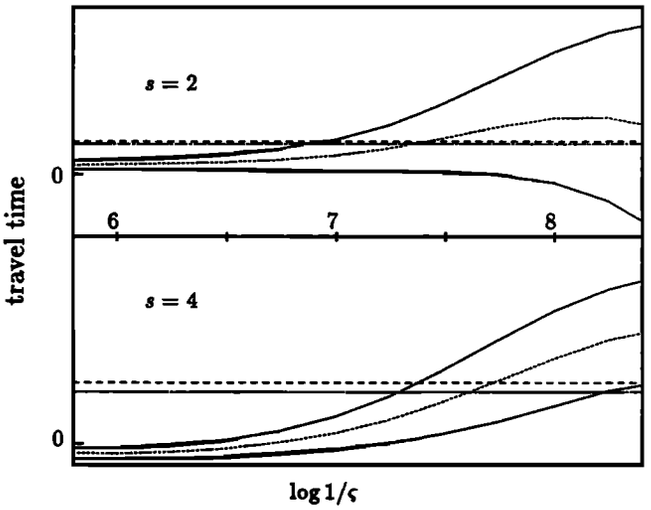

Fig. 4. Spherical harmonic expansion coefficients of degree $s = 2$ and 4 and order $t = 0$ of the travel time anomalies of antipodal *PKIKP* rays. Two horizontal lines are the results estimated by *Morelli et al.* [1986] (dashed line) and by *Shearer et al.* [1988] (dashed-dotted line) from ISC data. The dotted curve is the prediction from the inner core anisotropy model, which is inferred from the splitting functions of anomalously split core modes. The prediction is plotted as a function of the damping parameter ς, which is used in the damped least squares inversion for inner core anisotropy. The two solid curves above and below the prediction curve indicate the standard error estimates of the prediction.

and require $\log 1/\varsigma$ be between 7.4 and 8.3. Therefore the antipodal travel time data can be easily explained if the model has an appropriate size, say, corresponding to $\log 1/\varsigma$ equal to 7.4. Meanwhile the model corresponding to this damping level can aggregately fit the data of the core modes very well, 79% variance reduction can be achieved by the inner core anisotropy and model SAF together.

When we examine the fit of the resulting model to each individual mode, however, a serious problem appears. While the splitting function coefficients c_{20} of these core modes can be consistently explained by the model, this model is not able explain c_{40} of mode ${}_{13}S_2$. The reason for this becomes clear if we examine the kernel coefficients $\Psi_4^{(i)}$ (see (44)) of this mode and mode ${}_3S_2$ (the sensitivity of the latter mode to the inner core anisotropy is so strong that the main character of the model is determined by this mode alone to fairly large extent). For mode ${}_{13}S_2$, we have $\Psi_4^{(i)} =$ (28.6, -34.3, 7.8, 4.6, 3.2) x 10^{-3} ; and for mode ${}_3S_2$, $\Psi_4^{(i)}$ (26.8, -26.0, 6.6, 0.1, 1.4) x 10^{-2}. Clearly, it is very difficult to find a reasonable model $\psi_4^{(i)}$ which simultaneously explains the splitting function coefficients c_{40} of modes ${}_{13}S_2$ and ${}_3S_2$, which are equal to 1.9 x 10^{-3} and -3.8 x 10^{-3}, respectively.

The inconsistency of the splitting functions of these two modes could be interpreted in two ways. First the inner core anisotropy of the real Earth could more complicated than the form we assume here. The second possibility is that the reported splitting function coefficients of modes ${}_{13}S_2$, ${}_3S_2$, or both, which are retrieved by using the nonlinear least squares method, are not the true solution corresponding to the Earth. Anticipating some results presented below, we find that the split spectra of mode ${}_3S_2$ can, indeed, be explained by a totally different splitting function from the one tabulated in Table 3. This will be further discussed below.

5.3. *Modeling Split Modal Spectra*

Again we need to discuss the conditions under which the data error e can be treated approximately as samples from white noise so that $\mathbf{C}_e$ in (48) becomes proportional to identity matrix. In order to achieve this condition, we should in principle divide each row of the both sides of the basic equation in (47) by the expected size of the associated error of the data point. Generally speaking, errors in data have two sources: (1) observational noise (the noise level varies from spectrum to spectrum) and (2) unmodeled effects (e.g., the contributions from higher degrees of the spherical harmonic expansion and the coupling effects between adjacent modes, etc.). The latter could be incorporated into vector e and be regarded as "theoretical errors".

In paper 1 we have proposed the use of the seismogram before the event as the means for estimating the noise level for a given seismic trace. Dividing each trace by the estimated noise level, an arbitrary component of the error vector e in (47) can be written as $e_i^{ob} + e_i^{th}$, where e_i^{ob} are observational errors which have been normalized and have unit variance, and e_i^{th} are the "theoretical errors". Assuming the variance of e_i^{th} is λ_i^2, we only need divide each row of both sides of the equation by $\sqrt{1+\lambda_i^2}$ to make the error e white. Since we do not know the precise properties of "theoretical errors", we are forced to make assumptions. We shall assume that λ_i^2 are the same, all equal to λ_j^2, for all traces i belonging to the mode j and that they are proportional to the mean of the squared data amplitude $(\sum \tilde{d}_i^2/N_j)$, where the summation is over all data points i for the mode, $\tilde{d}_i$ are the data normalized by the estimated noise level, and N_j is the number of the data points of the mode j. It is further assumed that in the limit where the "theoretical errors" are dominant ($\lambda_j^2 \gg 1$), all modes (regardless of their data dimension N_j) have the same importance in controlling the model. (This implies that the "theoretical errors" of different data points for a given mode are not independent.) The idea can be formulated by assigning a multiplicative factor N_j to λ_j^2, which will be used to divide the both sides of the equation, to down-weight the modes having larger N_j. Combining the two factors, we have $\lambda_j^2 = \lambda^2 \sum \tilde{d}_i^2$, where λ^2 is a constant universal to all modes and the summation is over all data points i for the mode. λ^2 is a number related to the ratio of the variance of the "theoretical errors" and the variance of the observational errors. Due to the lack of enough information on these errors, we choose the number experientially. The number is chosen so that the data size of a mode (measured by $D^2 = \sum d_i^2$, where summation is over all data points i of the mode and d_i are the data which have been fully weighted) varies by a factor 5 from its minimum to maximum. For the relative data size of each mode, see Table 6.

Now let us describe what the model vector $\mathbf{x}$, introduced in (47), contains. Of course, the heterogeneity parameters ζ_{st}^k defined by (38) deserve the first consideration. As above, we truncate the spherical harmonic expansion at $S=4$ and the radial expansion at $K=6$. The topography of the CMB, represented by the spherical harmonic components of relative perturbation in the radius of the CMB (δh_{st}, $s = 0, 2, 4$), are retrieved simultaneously. The anomalously split modes

TABLE 6. Misfit to Each Mode of Model SAT and Splitting Functions

Mode	D^2	Var	Var′
${}_0S_3$	1.21	0.20	0.17
${}_0S_4$	0.74	0.40	0.32
${}_0S_5$	0.83	0.26	0.21
${}_1S_3 - {}_3S_1$	0.96	0.36	0.30
${}_0S_6$	1.26	0.18	0.14
${}_3S_2$	0.91	0.38	0.32
${}_1S_4$	1.03	0.36	0.33
${}_0S_7 - {}_2S_3$	1.63	0.25	0.13
${}_1S_5 - {}_2S_4$	1.25	0.49	0.34
${}_2S_5 - {}_1S_6$	1.21	0.84	0.73
${}_0S_9$	1.65	0.38	0.21
${}_1S_7$	1.00	0.41	0.28
${}_2S_6$	0.56	0.58	0.45
${}_1S_8$	1.07	0.46	0.31
${}_4S_3 - {}_2S_8$	1.22	0.68	0.45
${}_5S_3$	0.33	0.49	0.38
${}_4S_4$	0.42	0.68	0.54
${}_5S_4$	1.01	0.64	0.40
${}_5S_5$	1.13	0.44	0.35
${}_6S_3 - {}_3S_8$	0.85	0.59	0.35
${}_5S_6$	1.14	0.48	0.26
${}_9S_3$	0.82	0.70	0.44
${}_6S_{10}$	0.71	0.67	0.57
${}_{11}S_4$	0.97	0.68	0.40
${}_{13}S_2$	1.12	0.36	0.30
${}_{11}S_5$	1.02	0.81	0.55
${}_{13}S_3$	0.95	0.46	0.37
average	1.00	0.47	0.34

Squared data D^2 for each mode have been calculated from the weighted data (see text for details) and have been normalized so that their average is unity. Variance ratios (squared misfit/squared data) are listed for Model SAT (Var), see Table 7; and for splitting function coefficients (Var′), see Table 3. The average of Var and Var′ is weighted average with D^2 as weight.

will be modeled by inner core anisotropy; we include, in the vector $\mathbf{x}$, the parameters $\psi_s^{(p)}$ $(s = 0, 2, 4)$, introduced in (64). In section 5.2 we have pointed out that the current data are not sufficient to yield useful spherical corrections to the spherical reference model (PREM of *Dziewonski and Anderson* [1981]). However, significant perturbations in central frequencies and attenuation rates of many modes, as indicated by large coefficients A_0^0 and $\mathrm{Im}(A_0^0)$ in Table 3, require some parameters for spherical perturbations of the Earth model have to be included in the inversion to fit the modal spectra. We include the parameters $\alpha^{(k)}$, $\beta^{(k)}$, and $\rho^{(k)}$ (see (39), (40), and (41)) in the inversion. The corresponding Legendre expansions are truncated at $K = 3$. The parameters $\tilde{\mu}^{(k)}$ $(k = 0, 1, \ldots, 6)$ (see (46)) are also included in vector $\mathbf{x}$ to incorporate a spherical perturbation in mantle attenuation structure. The total dimension of the vector $\mathbf{x}$ is 150. We include these spherical perturbation parameters in the inversion, not because we intend to obtain a more precise spherical Earth model, but because the perturbations in central frequencies and in attenuation rates of the modes are coupled with aspherical effects and have to be modeled.

Having chosen the model space, we are now able to consider the specification of the model covariance matrix $\mathbf{C}_x$, which has been introduced in section 5.1. Since the parameter sets $\{\zeta_{st}^k\}$ in (38), $\{\delta h_{st}\}$ (spherical harmonic expansion coefficients of the relative perturbation in the radius of the CMB), and $\{\psi_s^{(p)}\}$ (see the appendix) are associated with some orthonormal bases, we may set all σ_i corresponding to $\{\zeta_{st}^k\}$ be σ_ζ, set all σ_i corresponding to $\{\delta h_{st}\}$ be σ_h, and set all σ_i corresponding to $\{\psi_s^{(p)}\}$ be σ_ψ. In evaluating the covariance matrix $\mathbf{C}_x$ for the linear inversion (see section 5.2), we described a strategy for choosing the value of σ_ζ/σ_h, which is also employed in the present case. In modeling the splitting functions of core modes, we were unable to find an inner core model of the form (64), which could fit all modes. However, the experiments that have been performed enable us gain some knowledge on the intensity of inner core anisotropy. Relying upon this kind of knowledge and the rms value of $\{\zeta_{st}^k\}$ of model SAF, we may choose a value of σ_ζ/σ_ψ for the current problem, which gives $\sigma_\zeta/\sigma_\psi = 0.01$. Although the parameters for spherical perturbations, $\alpha^{(k)}$, $\beta^{(k)}$, $\rho^{(k)}$ and $\tilde{\mu}^{(k)}$ (see (39), (40), (41), and (46), respectively) have been included in the model vector $\mathbf{x}$, the main interest of this study is in the aspherical structure of the Earth. For this reason we allow the parameters for the spherical perturbations move to wherever the data prefer, within the limits required by the stability of the inversion. Namely, we set elements σ_i corresponding to the parameters for the spherical perturbations to very large values relative to the other elements of $\mathbf{C}_x$.

In our inversion we have also used the results derived from antipodal *PKIKP* travel time data [*Morelli et al.*, 1986] as constraints on the inner core anisotropy $\psi_s^{(p)}$ (see (64)). We use the spherical harmonic coefficients of the travel time anomalies as the constraints $\mathbf{g}$ in (47). The reported travel time residuals have a cylindrically symmetric distribution with the symmetry axis coinciding with the Earth's rotation axis. Thus they provide two (for $s = 2, 4$ and $t = 0$) constraints on the model parameters $\psi_s^{(p)}$.

The result of the inversion is called SAT (Splitting data, Aspherical, from seismic Traces), and it is tabulated in Tables 7*a*–7*c*. The coefficients for the heterogeneity parameter $\zeta(r, \theta, \phi)$, see (38), and the CMB topography δh are listed in Table 7*a*. Table 7*b* tabulates the parameters, $\psi_s^{(p)}$, for inner core anisotropy, see (64). In Table 7*c* we list the coefficients for the spherical perturbations in P velocity (α), S velocity (β), density (ρ), and the imaginary part of the shear modulus in the mantle.

In Tables 7*a*–7*c* the associated standard errors of all of the model parameters and the corresponding diagonal elements of the resolution matrix are given. For the derivation and the reliability of these quantities, see section 5.1. One may immediately see that these error estimates are far too small. We ascribe the underestimate mainly to the damping of the model. The general deviation of the diagonal elements of the resolution matrix from unity (see Tables 7*a*–7*c*) indicates that the model is heavily damped. In such a case, the formal error analysis described above is very likely to lose meaning.

The misfit of this model, for each mode, is listed in Table 6. The misfit of a mode is defined by $\mathrm{Var} = \sum(d_i - d_i^P)^2/\bar{d}^2$, where d_i^P are the predicted values by SAT and $\bar{d}$ is the rms of the data d_i of the mode. We also list in Table 6 the misfits corresponding to the splitting functions tabulated in Table 3 using the same data. These misfits could be regarded as the minimum values which Earth models could achieve.

5.4. *Summary*

Inversions are performed by following two approaches: by inverting the splitting functions which have been retrieved

TABLE 7a. Model SAT, Part 1: Mantle Heterogeneity and CMB Topography

	${}^kA_0^0$	${}^kA_2^0$	${}^kA_2^1$	${}^kB_2^1$	${}^kA_2^2$	${}^kB_2^2$	${}^kA_4^0$	${}^kA_4^1$	${}^kB_4^1$	${}^kA_4^2$	${}^kB_4^2$	${}^kA_4^3$	${}^kB_4^3$	${}^kA_4^4$	${}^kB_4^4$
$k=0$	–	170	-69	68	-216	-262	23	-10	-17	64	39	-43	76	-51	63
	–	2	2	3	3	2	3	4	5	5	4	5	5	5	4
	–	0.73	0.79	0.76	0.66	0.66	0.64	0.64	0.60	0.58	0.60	0.52	0.53	0.48	0.48
$k=1$	–	-109	-11	-15	101	-4	17	-5	-31	-37	71	23	0	-6	-21
	–	3	5	4	0	2	4	4	4	4	4	4	3	3	3
	–	0.26	0.32	0.27	0.20	0.20	0.20	0.21	0.17	0.16	0.16	0.13	0.13	0.10	0.11
$k=2$	–	16	5	-11	45	-12	-18	13	-8	-57	6	49	-35	-15	17
	–	3	5	5	2	2	3	4	4	4	3	4	3	3	3
	–	0.24	0.27	0.24	0.17	0.16	0.15	0.16	0.14	0.13	0.14	0.11	0.12	0.08	0.09
$k=3$	–	60	-33	-37	-37	15	5	12	39	17	-34	-31	-1	35	0
	–	2	3	4	3	3	3	3	4	3	3	3	3	3	3
	–	0.16	0.18	0.17	0.11	0.12	0.13	0.11	0.12	0.09	0.09	0.07	0.07	0.08	0.07
$k=4$	–	-18	-33	-69	10	87	13	16	45	32	-13	-46	26	41	-37
	–	4	4	4	3	1	3	4	3	3	3	3	3	3	2
	–	0.16	0.19	0.15	0.12	0.12	0.11	0.12	0.10	0.08	0.09	0.07	0.07	0.07	0.07
$k=5$	–	-47	-26	-30	22	52	-26	20	21	20	-13	-13	16	3	-18
	–	2	3	3	2	3	3	3	3	2	2	2	2	3	2
	–	0.10	0.10	0.10	0.06	0.08	0.12	0.07	0.07	0.05	0.06	0.03	0.03	0.06	0.07
$k=6$	–	-38	-7	6	2	-12	-27	3	-5	-7	-11	5	-10	-5	5
	–	1	2	3	1	2	1	2	2	2	2	1	1	2	1
	–	0.04	0.05	0.07	0.02	0.03	0.05	0.03	0.04	0.03	0.03	0.02	0.02	0.02	0.03
$k=c$	379	-135	54	13	175	148	1	11	-1	16	68	16	21	45	-69
	17	11	12	12	10	10	8	10	9	9	9	11	11	8	8
	0.99	0.37	0.41	0.38	0.27	0.27	0.14	0.19	0.17	0.16	0.16	0.26	0.25	0.15	0.15

For convention see the legend to Table 4. Note that the spherical components of parameter $\zeta(r,\theta,\phi)$ are not defined due the failure of (37) for the spherical perturbations; for the spherical corrections in α, β, and ρ see Table 7c.

TABLE 7b. Model SAT, Part 2: Inner Core Anisotropy

	$\psi_s^{(1)}$	$\psi_s^{(2)}$	$\psi_s^{(3)}$	$\psi_s^{(4)}$	$\psi_s^{(5)}$	$\psi_s^{(6)}$	$\psi_s^{(7)}$
$s=0$	2.1	-2.9	0.9	-2.5	0.7	0.7	
	0.2	0.1	0.1	0.2	0.2	0.2	
	0.86	0.79	0.80	0.76	0.70	0.50	
$s=2$	-3.4	-1.7	1.8	4.3	0.1	-4.1	0.6
	0.1	0.1	0.1	0.2	0.2	0.2	0.2
	0.75	0.84	0.55	0.84	0.23	0.62	0.32
$s=4$	0.1	-3.7	0.0	-0.3	1.2		
	0.1	0.1	0.2	0.0	0.2		
	0.61	0.63	0.47	0.76	0.61		

Parameters $\psi_s^{(k)}$ (see (64)) are listed in the first entry for each spherical harmonic degree s in units of 10^{-2}. The estimates of standard errors are derived from the covariance matrix, and are given in the second entry for each s (in the same units). The third entry gives the corresponding diagonal elements of the resolution matrix. See text for details on the computation and the reliability of the error estimates.

from split spectra, the resulting model being named SAF and by inverting the split spectra directly, the resulting model being named SAT.

In the first approach, quantities of different spherical harmonic degrees and orders are decoupled from one another. This decoupling enables us to model the aspherical part of the splitting functions only, without needing to model the splitting function coefficients of degree 0, which are not expected to have enough resolution to yield reliable spherical corrections to the reference Earth model. The splitting functions of the mantle modes are well modeled by mantle heterogeneity and CMB topography. The residuals of the splitting functions of core modes from the mantle model are very large, and are further modeled by inner core anisotropy. The modeling fails to explain each individual splitting function coefficient of the core modes.

In the second approach, a model is sought to optimally fit the observed modal spectra. All the model parameters have to be determined simultaneously. The inversion is nonlinear and is performed iteratively. The resulting model SAT includes mantle heterogeneity, CMB topography, and inner core anisotropy. Spherical correction parameters are also included in the inversion, to absorb the perturbations in central frequencies and in attenuation rates of the multiplets. The purpose of this experiments is to determine if we are able to develop a relatively simple Earth model which can fit the observed modal spectra and thus to investigate po-

TABLE 7c. Model SAT, Part 3: Spherical Mantle Perturbations in α, β, ρ, and Imaginary Part of Shear Modulus

	$k=0$	$k=1$	$k=2$	$k=3$	$k=4$	$k=5$	$k=6$
$\alpha^{(k)}$	-62	-198	-403	-433			
	17	28	23	26			
	0.82	0.59	0.39	0.30			
$\beta^{(k)}$	-415	356	749	-25			
	20	29	28	23			
	0.78	0.53	0.56	0.23			
$\rho^{(k)}$	217	-844	545	-565			
	17	30	20	22			
	0.10	0.41	0.22	0.24			
$\bar{\mu}^{(k)}$	132	417	268	368	-166	-170	-447
	25	61	68	69	67	66	54
	0.96	0.73	0.63	0.47	0.46	0.35	0.18

Use (39), (40), (41), and (46) to calculate the spherical perturbations in α, β, ρ, and the imaginary part of shear modulus, respectively. The coefficients are listed in the first entry for each parameter, $\alpha^{(k)}$, $\beta^{(k)}$, $\rho^{(k)}$, and $\bar{\mu}^{(k)}$, in unit of 10^{-6}. The associated standard errors estimated from the covariance matrix are listed in the second entry for each parameter in the same units. In the third entry are listed the corresponding diagonal elements of the resolution matrix. See text for details on the computation and the reliability of the error estimates.

tential biases in the splitting functions, which could be the cause of the failure in developing a successful model of inner core anisotropy by following the first approach.

Both models SAF and SAT are further discussed and compared with some independent Earth models in the next section.

6. EARTH MODELS

6.1. *Heterogeneity in the Mantle*

In Figures 5–11, four different mantle models are shown at depths of 300, 500, 700, 1200, 1700, 2200, and 2700 km: (*a*) model SAT, modal model retrieved directly from seismic traces; (*b*) model SAF, modal model retrieved from splitting functions; (*c*) model SW, based on waveform studies on *SH* body waves [*Woodhouse and Dziewonski*, 1986]; and (*d*) model M84A (for the upper mantle) [*Woodhouse and Dziewonski*, 1984] or model V.3 (for the lower mantle) [*Morelli and Dziewonski*, 1987*b*]. To be comparable with the other models, *P* velocity model V.3 has be multiplied by a factor 2 when it is presented in Figures 7*d*–11*d*.

First of all, great similarities between models SAT and SAF are evident at all depths. This verifies that the inversion results for the splitting functions of the mantle modes, as given in Table 3, are mutually consistent. This consistency provides evidence (which is more compelling than the formal error estimates) that the splitting functions have been successfully retrieved and that they do, indeed, reflect the Earth's three-dimensional structure.

Upper mantle heterogeneity, as revealed by waveform studies [*Woodhouse and Dziewonski*, 1984; 1986], varies with depth relatively rapidly. For example, both models SW and M84A exhibit a dramatic change in the depth range 300–500 km (Figures 5 and 6). Naturally the splitting of low-frequency normal modes is sensitive to larger-scale structures. Thus it may not be appropriate to expect that the modal models, retrieved from the current data set, could have sufficient resolution to recover the rapid radial variation in the upper mantle. We should be satisfied if the models can represent the very large-scale features of the upper mantle. Our resulting models, SAF and SAT, are, indeed, correlated with the models based on the waveform studies. The correlation coefficients between, for example, the modal model SAF and the *SH* waveform model SW is above 0.5 (corresponding to 95% significance level) for most of the upper mantle, except in the region near depth of 500 km where the correlation coefficient is still positive. The strong similarity in pattern between SAT and SW at 300 km depth (Figures 5*a* and 5*c*) further confirms that the modal models do bear important signals from the upper mantle. The inversion results indicate that the data set used in this study is sensitive mostly to the lower mantle structure. While the damping level we used makes the modal models too small for the upper mantle, as compared with waveform models, the results for the lower mantle are in agreement with our knowledge based other existing models, e.g., model SW and travel time model V.3 of *Morelli and Dziewonski* [1987*b*].

The agreement in the lower mantle among modal models SAT and SAF, *SH* waveform model SW, and *P* travel time model V.3 is remarkable. At the depth interval between 2000 and 2700 km, the agreement is almost perfect: correlation coefficients are around 0.9, corresponding to 100% significant level. The excellent agreement extends up to the depth of 1300 km between the modal models and the waveform model. The travel time model V.3 is highly consistent in pattern with the other models between depths of 1000 km and 2000 km, but it has a very small amplitude from the depth of 1600–1900 km, relative to the other models (cf. Figure 9). The discrepancy of these models at the top of the lower mantle (say, see Figure 7) may be largely attributed to the following facts. The aliasing from the strong heterogeneity in the upper mantle is expected for all models, especially the modal models (e.g., comparing Figures 5*a*–7*a*). The horizontal resolution of the travel time model V.3 may also be poor in this region (A. M. Dziewonski, personal communication, 1988).

Our main interest in this study is focused on the aspherical structure of the Earth. In order to investigate the contamination to our results due to the potential spherical deviation from the reference starting model, however, we have simultaneously included spherical corrections (for velocities, density, and attenuation) in our inversion. The correction results are list in Table 7*c*. The sizes of these corrections are small, though no damping is applied on these parameters (we adopt this strategy so that spherical perturbations can absorb the data residuals as much as possible). These spherical correction parameters are somewhat helpful in reducing the data variance. This indicates that although the spherical reference model (PREM of *Dziewonski and Anderson* [1981]) can predict the central frequencies of normal modes fairly well (with errors smaller than splitting widths), it needs corrections when the structure of singlets is studied. (The splitting width of a multiplet is defined as the frequency difference between the singlet with highest frequency and the singlet with the lowest frequency.) Unfortunately, the data employed here cannot yield useful spherical corrections to the PREM model. For this a much larger data set is needed.

6.2. *Topography of the Core-Mantle Boundary*

We realize that the trade-off between our CMB topographic models and volumetric mantle models is strong. Therefore we do not intend to use these CMB models to challenge existing models. Nevertheless, it is interesting to compare the modal results with those of previous studies. In Figure 12 we show four topography models for the core-mantle boundary: (*a*) the modal model SAT, and (*b*) the modal model SAF; for comparison the CMB model X222 of *Morelli and Dziewonski* [1987*a*] is also shown in Figure 12: (*c*) the filtered version of X222 with only even degrees and (*d*) the complete model with both even and odd degrees. Model X222, inferred from *PcP* and PKP_{BC} travel times anomalies, has large odd-degree components, evident in Figure 12. Since the data distribution of travel times is uneven (see Figures 3 and 5 of *Morelli and Dziewonski* [1987*a*]), it is possible that aliasing between even- and odd-degrees terms may occur. The travel time sampling is relatively poor under the Africa–Indian-Ocean–Australia region (see Figures 3 and 5 of *Morelli and Dziewonski* [1987*a*]). If this region is ignored, implying that model X222 could become a model dominated by even-degree components, similarities between the modal models and the unfiltered X222 model in Figure 12 are evident. The modal models are smaller than the travel time model by a factor of the order of 2. This could be attributed to the trade-off between the CMB structure and the lower mantle perturbation for the modal models.

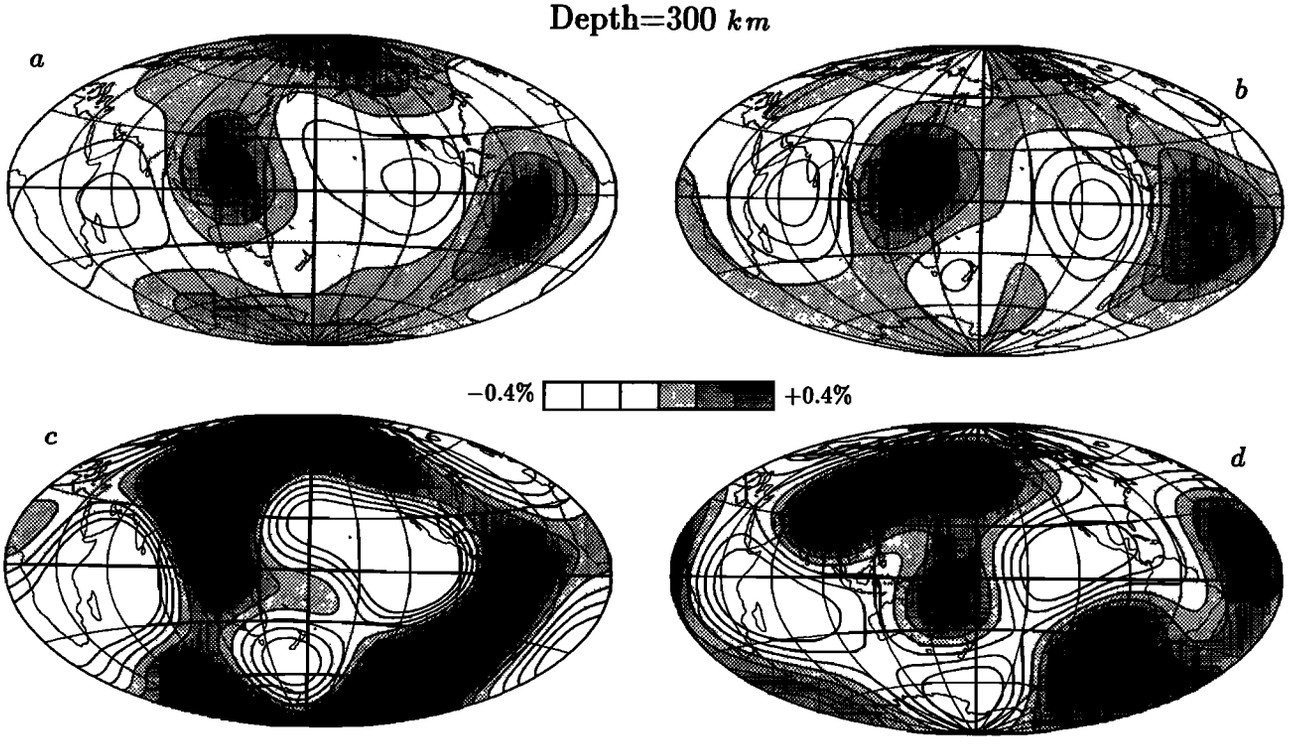

Fig. 5. Maps of heterogeneity in the mantle of spherical harmonic degree $s = 2$ and 4 only. (*a*) v_S perturbation of model SAT, retrieved directly from the split spectra of free oscillations from which splitting functions of some modes have been inferred; (*b*) v_S perturbation of model SAF, retrieved from splitting functions; (*c*) model SW, a *S* velocity model based on waveform study of *SH* body waves by *Woodhouse and Dziewonski* [1986]; (*d*) model M84A, a *S* velocity model based on waveform study of mantle waves by *Woodhouse and Dziewonski* [1984].

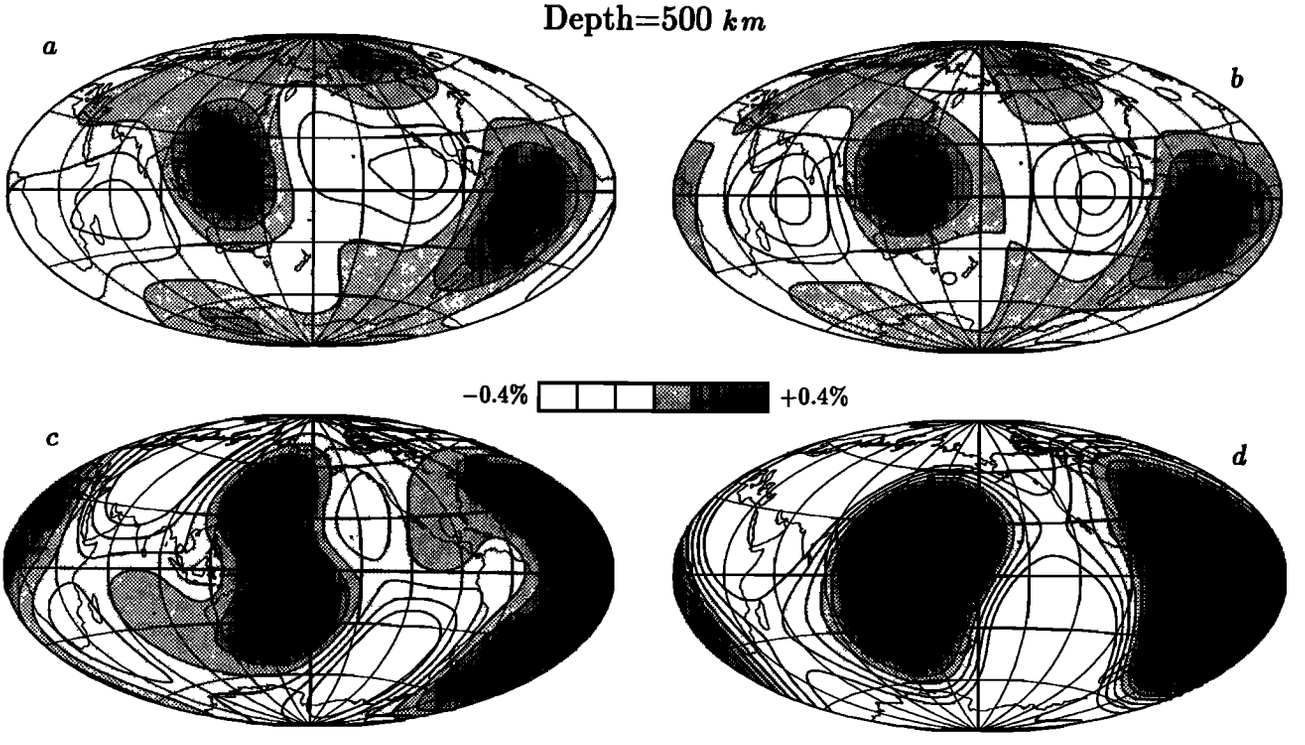

Fig. 6. Maps of heterogeneity in the mantle of spherical harmonic degree $s = 2$ and 4 only. See caption to Figure 5.

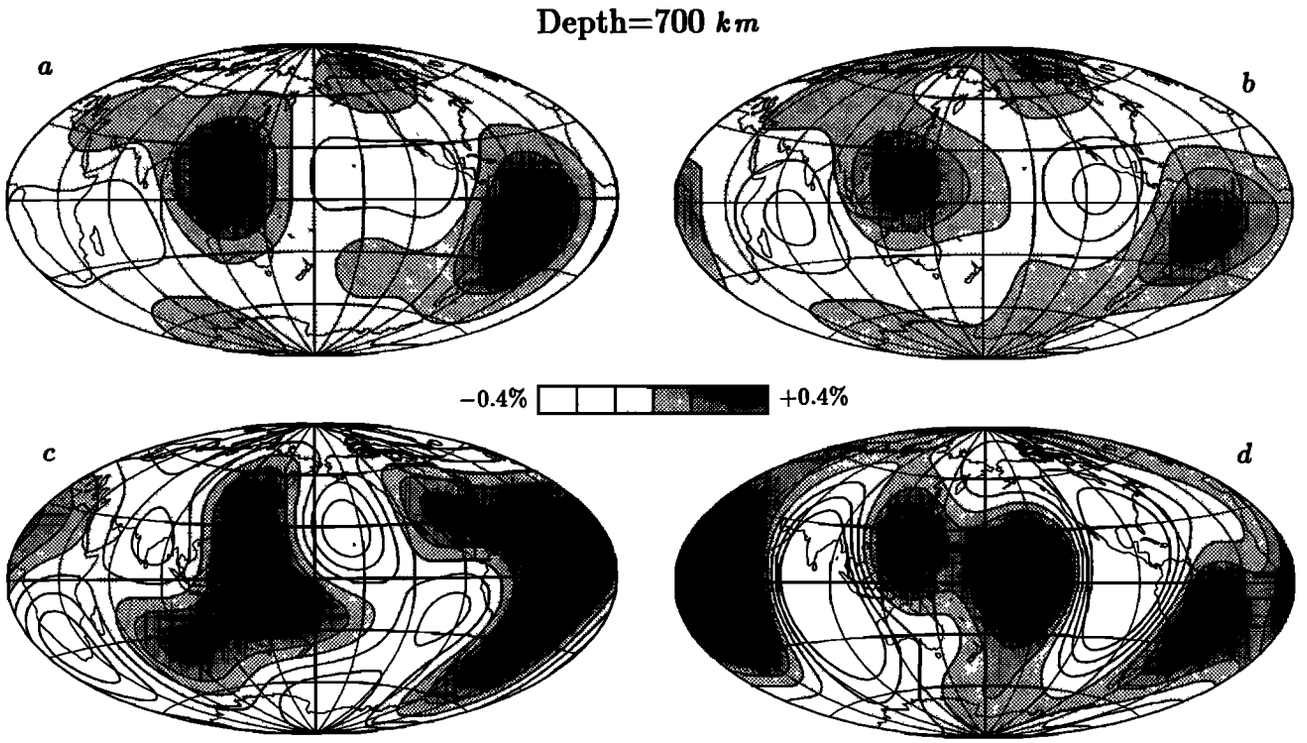

Fig. 7. Maps of heterogeneity in the mantle of spherical harmonic degree $s = 2$ and 4 only. See caption to Figure 5 with exceptions that Figure 7(d) is replaced by $2\times$ v_P perturbation of model V.3, a model based P travel time residuals by *Morelli and Dziewonski* [1987*b*].

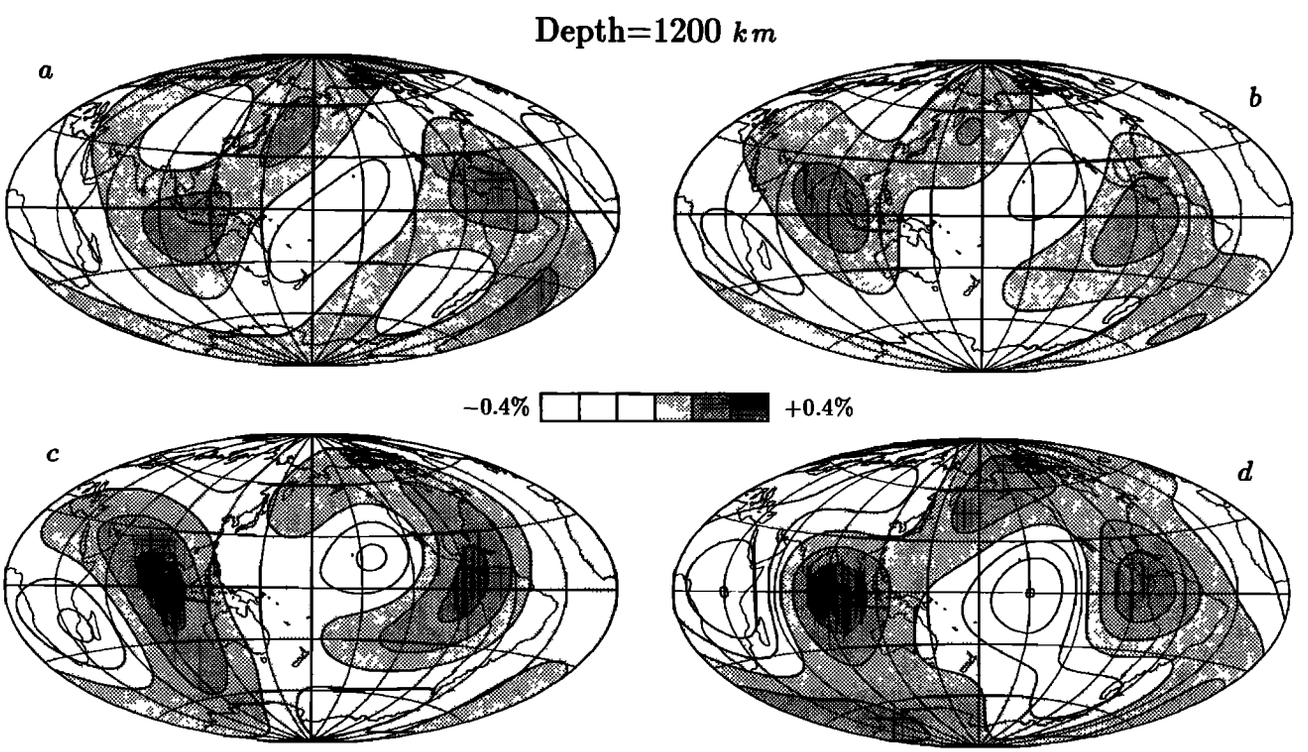

Fig. 8. Maps of heterogeneity in the mantle of spherical harmonic degree $s = 2$ and 4 only. See caption to Figure 7.

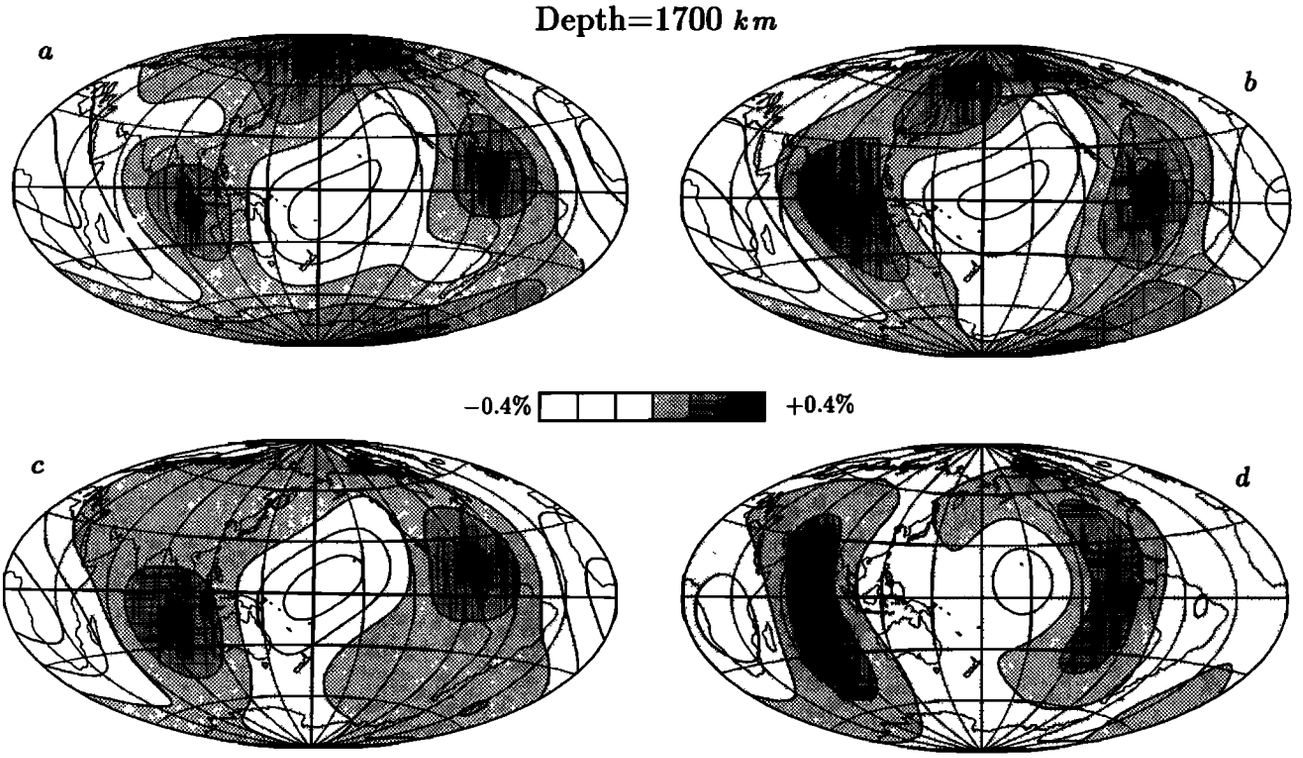

Fig. 9. Maps of heterogeneity in the mantle of spherical harmonic degree $s = 2$ and 4 only. See caption to Figure 7.

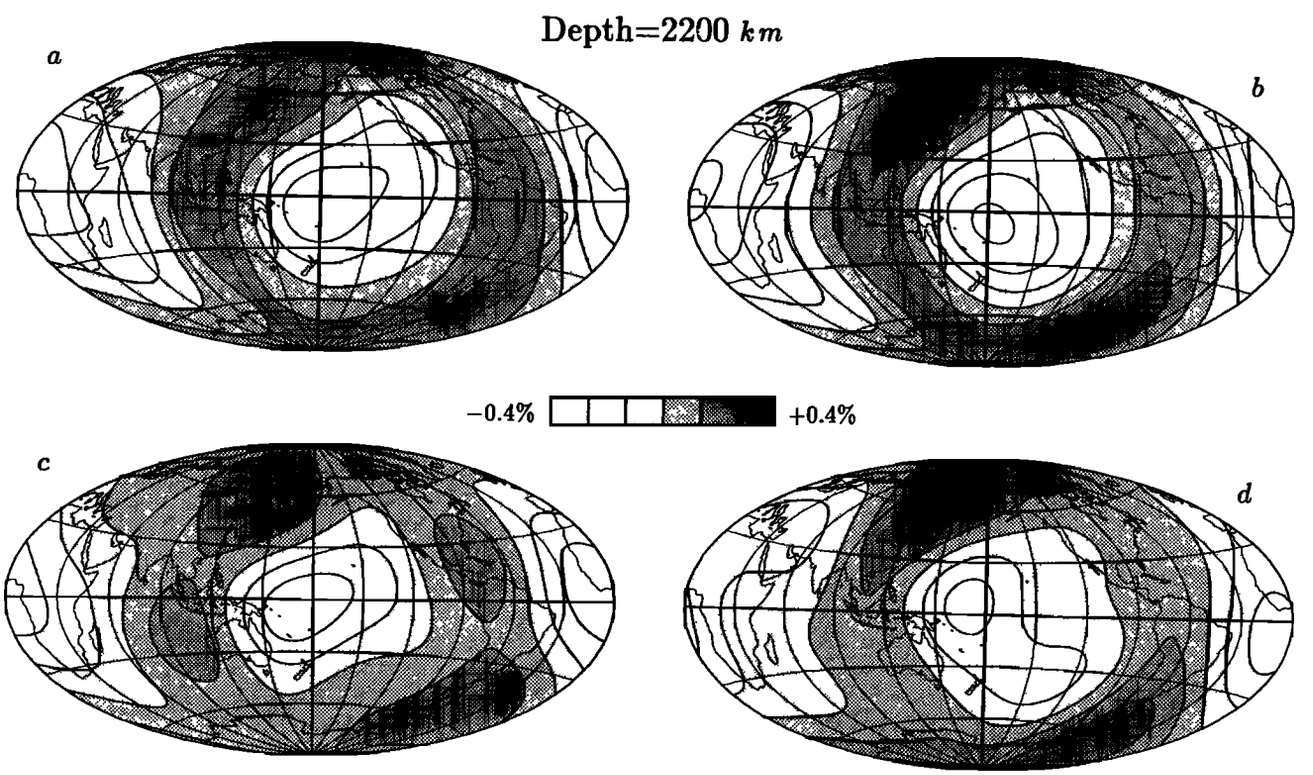

Fig. 10. Maps of heterogeneity in the mantle of spherical harmonic degree $s = 2$ and 4 only. See caption to Figure 7.

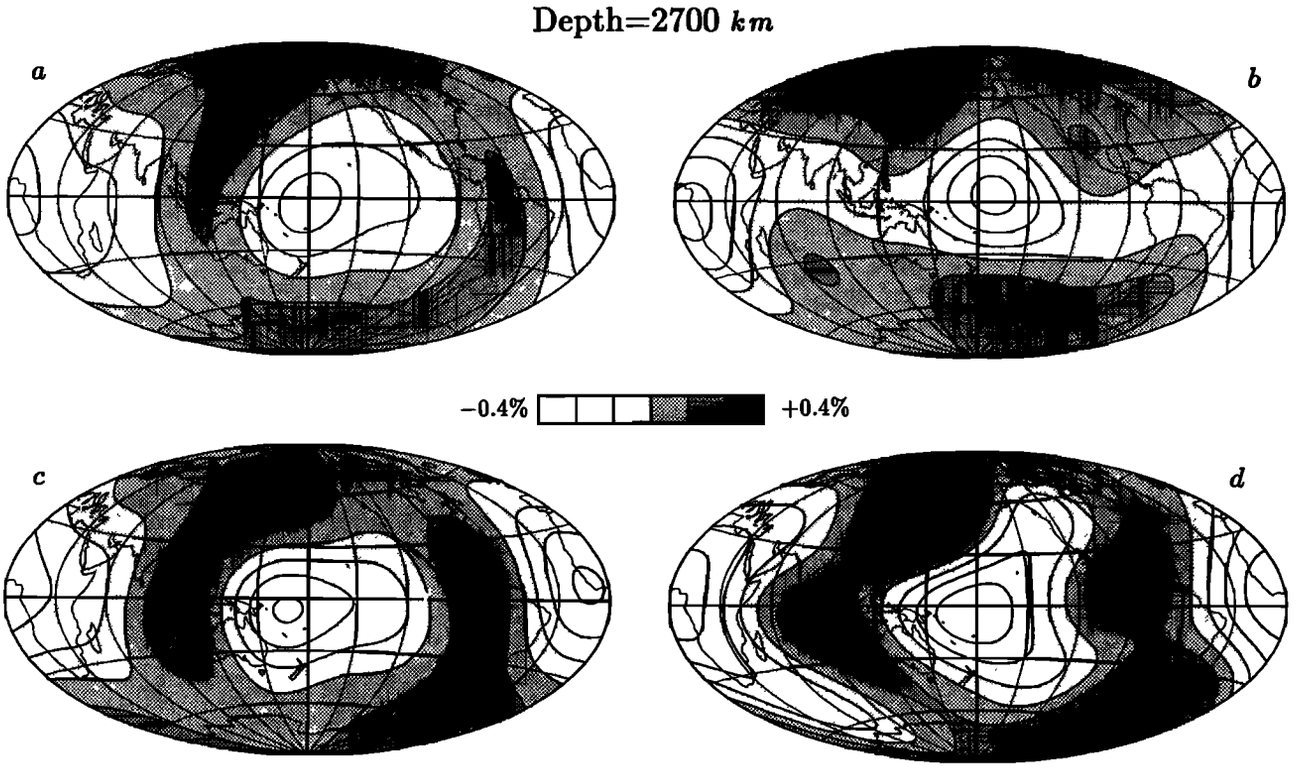

Fig. 11. Maps of heterogeneity in the mantle of spherical harmonic degree $s = 2$ and 4 only. See caption to Figure 7.

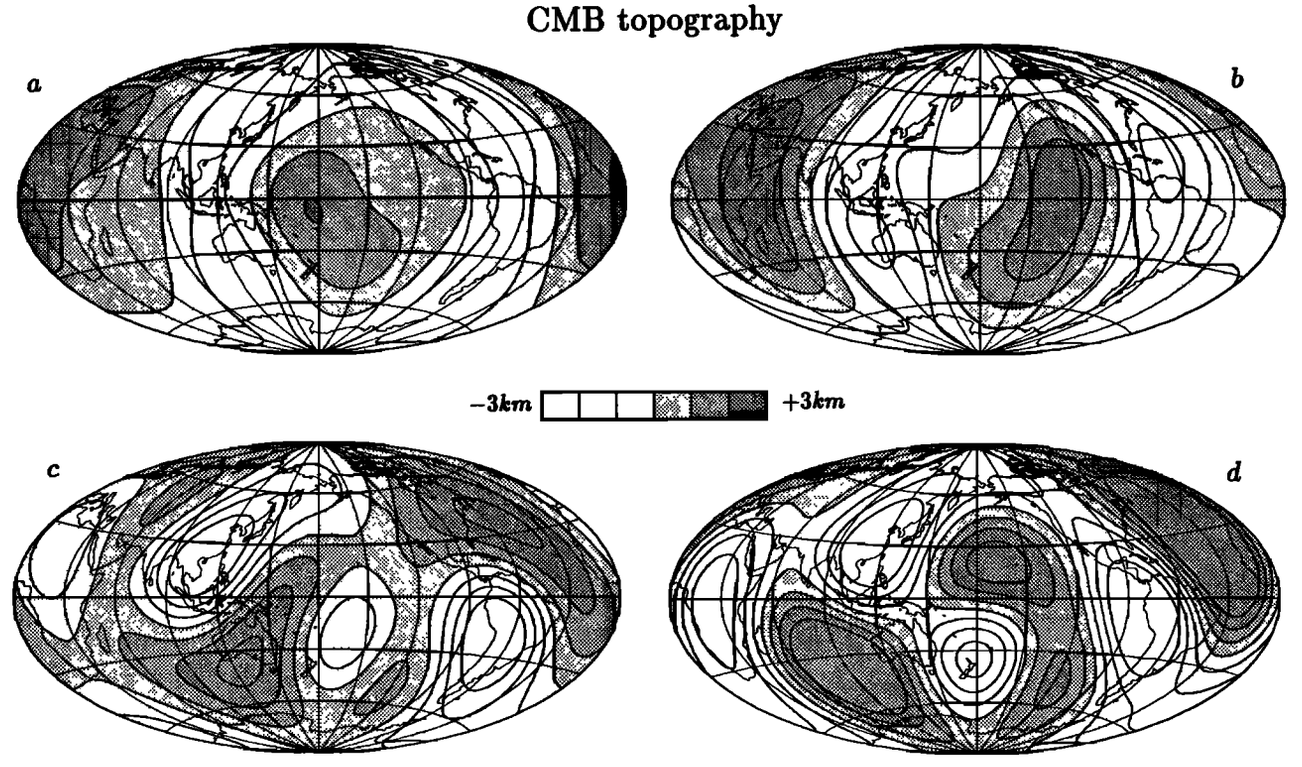

Fig. 12. Maps of topography models of the core-mantle boundary. (*a*) Model SAT, retrieved directly from the split spectra of the free oscillations from which splitting functions of some modes have been inferred; (*b*) model SAF, retrieved from splitting functions; (*c*) the even-degree part of the model by *Morelli and Dziewonski* [1987*a*]; (*d*) the full model (with both even and odd degrees) of *Morelli and Dziewonski* [1987*a*] constrained by PcP and PKP_{BC} travel times.

It is also interesting that the modal CMB models are qualitatively consistent with the dynamic predictions from mantle-convection models (e.g., *Richards and Hager* [1984]). This is indicated by the fact that the areas perturbed upwards on the CMB are systematically associated with the low-velocity regions in the mantle.

In summary, the inversion results for the CMB topographic models do not conflict with but can yield independent confirmations of, our current understanding of the shape of the CMB.

6.3. *Core Modes and Inner Core Anisotropy*

Since the inversion for the inner core anisotropy is an underconstrained inverse problem, we do not expect to find the unique solution from our data set (eight core modes only). Instead, we seek to demonstrate that inner core anisotropy can provide an explanation for the behavior of the anomalously split core modes, which have not been successfully modeled using other hypotheses. Here we shall address two questions: (1) how well does model SAT, which includes the inner core anisotropy, fit the data for core modes? and (2) can the model predict the *PKIKP* travel time anomalies?

In attempting to explain the zonal part of splitting function of the core modes, we were unable to derive a relatively simple model of inner core anisotropy to fit the splitting function coefficients listed in Table 3 (see section 5.2). The anisotropic inner core model of SAT, however, is required to optimally fit the original seismic trace from which the splitting functions have been retrieved. It is interesting, therefore, to see to what extent the predicted zonal parts of the splitting functions of the core modes agree with those retrieved for individual mode. In Table 8 the predicted c_{20} and c_{40} of eight core modes are tabulated together with those retrieved from the split spectra.

TABLE 8. Comparison of Predicted and Retrieved c_{20} and c_{40} of Core Modes

Mode	c_{20}		c_{40}	
	predicted	retrieved	predicted	retrieved
${}_3S_2$	205	52	99	-38
${}_{13}S_2$	39	34	14	19
${}_6S_3$	40	39	7	14
${}_2S_3$	40	54	4	6
${}_{13}S_3$	32	31	0	0
${}_9S_3$	25	5	-5	-12
${}_{11}S_4$	24	25	1	5
${}_{11}S_5$	15	25	0	4

Splitting function coefficients c_{20} and c_{40} predicted from model SAT are listed in the columns titled "predicted"; and those retrieved from the seismograms are listed in the columns titled "retrieved". All are in units of 10^{-4}.

We can see immediately that the predicted c_{20} and c_{40} of mode ${}_3S_2$ by model SAT do not agree with those retrieved from the seismograms at all. However, model SAT does explain fairly well the original split spectra from which the splitting function has been derived, as indicated by ratio Var/Var′, where Var and Var′ are listed in Table 6. The ratio for mode ${}_3S_2$ is 1.19, better than the average value for all the modes together. Therefore we are convinced that there is more than one splitting function, possibly a sequence of them, which can explain the spectral splitting of mode ${}_3S_2$ essentially equally well for the current data. We suspect that this nonuniqueness may be attributed largely to the highly nonlinear relationship, as indicated by the large predicted c_{20} and c_{40} coefficients (see Table 8), between the seismograms and the splitting function of mode ${}_3S_2$. The splitting function predicted by model SAT is favored over the one listed in Table 3, owing to its consistency with splitting functions of other modes.

The retrieved c_{20} and c_{40} of the other core modes can be explained very well by the anisotropic inner core model, an overall 90% variance reduction is achieved if mode ${}_3S_2$ is excluded. Therefore we may conclude that the anisotropic inner core model, part of model SAT, is a model which can explain the anomalous splitting of core modes.

Now let us turn our attention to the predicted *PKIKP* travel times of model SAT. In order to fit the travel time data, two efforts have been made in the inversion: (1) a priori level of intensity of inner core anisotropy has been chosen to be consistent with the travel time observations; and (2) antipodal *PKIKP* travel time data are strictly imposed as constraints in the inversion. As a result, model SAT predicts practically the same antipodal *PKIKP* travel times as do the models of *Morelli et al.* [1986] and *Shearer et al.* [1988], though they represent very different anisotropic fields (see Table 9). In an attempt to reduce the discrepancy between the results derived from travel time anomalies and those derived from modal splitting, *Morelli et al.* [1986] introduced a radial dependence proportional to r^2 in the inner core anisotropic parameters. This model is still not successful in modeling modal results and, furthermore, *Shearer et al.* [1988] point out that this model predicts overly large

TABLE 9. Comparison of Inner Core Anisotropic Models

	Model	$\psi_s^{(1)}$	$\psi_s^{(2)}$	$\psi_s^{(3)}$	$\psi_s^{(4)}$	$\psi_s^{(5)}$	$\psi_s^{(6)}$	$\psi_s^{(7)}$	Travel Time Coefficients t_s
	SAT	2.1	-2.9	0.9	-2.5	0.7	0.7		
$s=0$	*MDW*	1.17		0.51					$-.387\psi_0^{(1)} + .394\psi_0^{(3)} + .333\psi_0^{(5)}$
	STO	.77							
	SAT	-3.4	-1.7	1.8	4.3	0.1	-4.1	0.6	$.293\psi_0^{(1)} - .298\psi_0^{(3)}$
$s=2$	*MDW*	-4.95		-2.16					$-.113\psi_0^{(5)} - .178\psi_0^{(6)}$
	STO	-2.58							
	SAT	0.1	-3.7	0.0	-0.3	1.2			$-.138\psi_0^{(1)} + .141\psi_0^{(2)}$
$s=4$	*MDW*	7.51	3.28						$+.080\psi_0^{(3)} + .178\psi_0^{(4)}$
	STO	3.52							

In order to compare our inner core anisotropic model with the models of *Morelli et al.* [1986] (*MDW*) and of *Shearer et al.* [1988] (*STO*), we here express these two models in terms of the parameters $\psi_s^{(k)}$ (see (64)), in units of 10^{-2}. The antipodal *PKIKP* travel time residuals, δt, can be calculated from $\delta t = T(t_0 Y_0^0 + t_2 Y_2^0 + t_4 Y_4^0)$, where T is the travel time predicted by the spherical reference model (PREM of *Dziewonski and Anderson* [1981]), and $Y_s^t = Y_s^t(\theta, \phi)$ are completely normalized spherical harmonics as defined by *Edmonds* [1960] with θ and ϕ being the polar coordinates of the point where the ray intersects with the inner core boundary.

travel time anomalies for rays which turn at shallow depths in the inner core. In Figures 5, 6, and 7 of *Shearer et al.* [1988], they show the average travel time anomalies, observed and predicted by some models, as a function of the depth of the turning point and of the ray angle from the rotation axis of the Earth. Such averages are sensitive to inner core anisotropy. In order to make a comparison with these results, we plot the predictions of the model SAT in Figure 13. Clearly, the problem of overly large travel time anomalies, shown in Figure 6 of *Shearer et al.* [1988], is overcome by the model SAT.

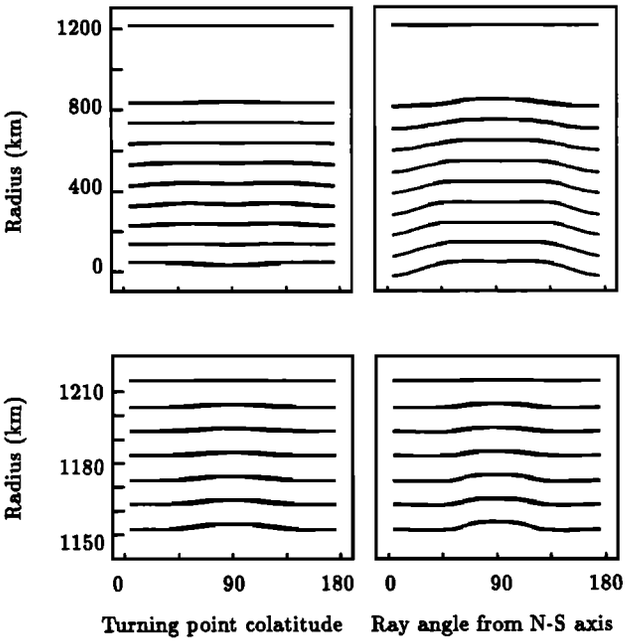

Fig. 13. Predictions from model SAT of the averaged *PKIKP* travel time anomalies, as a function the turning point of the ray, which is characterized by is depth and colatitude (left panels) or the ray angle from the rotation axis (right panels). This figure should be compared with Figures 5 and 6 of *Shearer et al.* [1988], which show too large predicted anomalies by a particular model of inner core anisotropy of [*Morelli et al.*, 1986]. For the observed anomalies see Figures 3, 6, and 7 of *Shearer et al* [1988]. The scaling is as by *Shearer et al* [1988]: 3 s is equivalent to 100 km in the upper panels and 1 s is equivalent to 6 km in the lower panels.

In summary, the inner core anisotropy of model SAT is an example of a model which successfully explains the splitting of anomalously split modes and simultaneously predicts *PKIKP* travel time anomalies fairly well.

7. CONCLUSIONS

We have derived large-scale, three-dimensional Earth models from the information contained in split spectra of free oscillations. The results are essentially consistent with preexisting heterogeneous Earth models based upon independent data and techniques, indicating that heterogeneity in the seismic velocities is, at most, weakly dependent on frequency. This consistency is very encouraging and demonstrates the ability to obtain models of Earth structure spanning 3 orders of magnitude in frequency.

The inversions have been performed by following two approaches: by inverting the splitting functions which have been retrieved from split spectra and by inverting the split spectra directly. The results obtained by these two methods are very much the same for the mantle structure. Thus it is shown that splitting functions can serve as a convenient intermediate step in inferring Earth models from splitting of the normal modes. With the current data set, most splitting functions retrieved can be consistently explained by relatively simple three-dimensional models of the mantle, together with a zonally anisotropic inner core. Modeling has revealed that the split spectra of a few multiplets (${}_3S_2$ is the most serious case) can be fit by very different splitting functions. This nonuniqueness should be overcome, we believe, when more data are available.

In order to explain the anomalous splitting behavior of the core modes, we are forced to introduce inner core anisotropy. Under the constraint that the anisotropic field has no singularities at the center of the Earth, we have developed a relatively simple model of inner core anisotropy, which can explain both the anomalous splitting of the core modes and the *PKIKP* travel time data.

The technique presented in this study provides a very encouraging prospect for the study of normal modes. It is straightforward to generalize the technique to include the coupling of different multiplets. This will make it possible to employ much more data, to study the splitting and the coupling of many new modes, and to constrain odd-degree structure of the Earth. The new networks currently under development [*Romanowicz et al.*, 1984; *Nolet et al.*, 1985; *Smith*, 1986; *Romanowicz and Dziewonski*, 1986] will make it possible to study splitting function coefficients of higher degrees and will provide better constrained results. Some very important geophysical problems which cannot be solved today, such as that of constraining the lateral heterogeneity in density of the mantle, will eventually have reliable solutions.

APPENDIX

It can be shown [*Woodhouse and Li*, 1990] that an elastic tensor field $\mathbf{L}$ which is analytic in the unit sphere centered at the origin may be expressed

$$\mathbf{L} = \sum_{s,t} \sum_{k=1}^{5} \sum_{n=\Delta s}^{s+s_k} \sum_{q=0}^{\mathrm{ent}\frac{n}{2}} \psi_{kst}^{(nq)} \tau_{kst}^{(nq)}(r,\theta,\phi) \qquad (58)$$

where $\Delta s = |s - s_k|$, $(s_1, s_2, s_3, s_4, s_5) = (4, 2, 2, 0, 0)$, $\tau_{kst}^{(nq)}$ are known basis tensors, $\psi_{kst}^{(nq)}$ are expansion coefficients, and

$$\mathrm{ent}\frac{n}{2} = \begin{cases} \frac{n}{2} & \text{if } n \text{ is even} \\ \frac{n-1}{2} & \text{if } n \text{ is odd} \end{cases} \qquad (59)$$

The basis tensor fields satisfy the orthonormality relation

$$\int \tau_{kst}^{(nq)*} \cdot \tau_{k's't'}^{(n'q')} dv = \delta_{ss'}\delta_{tt'}\delta_{kk'}\delta_{nn'}\delta_{qq'} \qquad (60)$$

where the volume integration is over the interior of the unit sphere and asterisk denotes complex conjugation, and have spherical contravariant components [*Phinney and Burridge*, 1973]

$$\tau_{kst}^{(nq)\alpha\beta\gamma\delta} = C_{knqs}^{\alpha\beta\gamma\delta}(r)\widehat{Y}_s^{Nt}(\theta,\phi) \tag{61}$$

where $C_{knqs}^{\alpha\beta\gamma\delta}$ are given below and $\widehat{Y}_s^{Nt}$, with $N = \alpha+\beta+\gamma+\delta$, are generalized spherical harmonics satisfying (14). Coefficients $C_{knqs}^{\alpha\beta\gamma\delta}$ may be calculated from

$$\begin{aligned} C_{knqs}^{\alpha\beta\gamma\delta} &= \alpha_{kN}^{\alpha\beta\gamma\delta}(2n+1)^{\frac{1}{2}}(-1)^N \begin{pmatrix} s_k & n & s \\ -N & 0 & N \end{pmatrix} \\ &\times\ r^n(4q+2n+3)^{\frac{1}{2}}P_q^{(0,n+\frac{1}{2})}(2r^2-1) \end{aligned} \tag{62}$$

where $\alpha_{kN}^{\alpha\beta\gamma\delta}$ are obtainable from Table 10, the Wigner 3-j symbols are defined by *Edmonds* [1960], and the functions $P_q^{(0,n+\frac{1}{2})}(2r^2-1)$ are the Jacobi polynomials [*Abramowitz and Stegun*, 1965] which are given by

$$\begin{aligned} P_q^{(0,n+\frac{1}{2})}(2r^2-1) &= \frac{1}{\Gamma(q+1)}\sum_{j=0}^{q}(-1)^{q-j}\begin{pmatrix} q \\ j \end{pmatrix} \\ &\times\ \frac{\Gamma(n+q+j+3/2)}{\Gamma(n+j+3/2)}r^{2j} \end{aligned} \tag{63}$$

Now let us seek an inner core tensor field $\mathbf{\Lambda}$ satisfying (30), which is equivalent to excluding all $\tau_{kst}^{(nq)}$ with $n+s$ odd from the expansion of $\mathbf{\Lambda}$. We assume that $\mathbf{\Lambda}$ is cylindrically symmetric about the Earth's rotation axis and has only even degrees up to $s = 4$ in its spherical harmonic expansion. We also assume that $\mathbf{\Lambda}$ varies smoothly with radius and has only the terms associated with r^0, r^1, and r^2 remaining in the radial expansion (equivalent to imposing the constraint $n + 2q \geq 2$). The final constraint which we place on $\mathbf{\Lambda}$ is that the inner core does not have lateral variations in Lamé coefficients, which can be expressed as $\psi_{4st}^{(nq)} = \psi_{5st}^{(nq)} = 0$ for $s \neq 0$. Under these constraints, $\mathbf{\Lambda}$ has only 18 degrees of freedom. Specifically, we write

$$\mathbf{\Lambda} = C(r)\Big(\sum_{p=1}^{6}\psi_0^{(p)}\lambda_0^{(p)} + \sum_{p=1}^{7}\psi_2^{(p)}\lambda_2^{(p)} + \sum_{p=1}^{5}\psi_4^{(p)}\lambda_4^{(p)}\Big) \tag{64}$$

where $C(r) = \kappa(r) + \frac{4}{3}\mu(r)$ is evaluated in the reference model (r is normalized such that $r = 1$ at the inner core boundary), $\psi_s^{(p)}$ are dimensionless coefficients to be determined, and $\lambda_s^{(p)} = \tau_{ks0}^{(nq)}$ with (k,n,q) taking the values listed in Table 11. The basis tensors $\lambda_s^{(p)}$ may also be expressed in terms of their spherical components $\lambda_{ijkl}^{(sp)}$:

$$\lambda_s^{(p)} = \sum_{ijkl}\lambda_{ijkl}^{(sp)}\mathbf{e}_i\mathbf{e}_j\mathbf{e}_k\mathbf{e}_l \tag{65}$$

TABLE 11. Values of Triplets (k,n,q) for Some (s,i)

	$s=0$	$s=2$	$s=4$
$i=1$	4,0,0	2,0,0	1,0,0
$i=2$	5,0,0	3,0,0	1,0,1
$i=3$	4,0,1	2,0,1	1,2,0
$i=4$	5,0,1	3,0,1	2,2,0
$i=5$	2,2,0	1,2,0	3,2,0
$i=6$	3,2,0	2,2,0	
$i=7$		3,2,0	

TABLE 10. Coefficients $\alpha_{kN}^{\alpha\beta\gamma\delta}$

		α	β	γ	δ	w_{Ni}	d_{kNi} $k=1$	$k=2$	$k=3$	$k=4$	$k=5$
$N=4$	$i=1$	+	+	+	+	1	1				
$N=3$	$i=1$	+	+	+	0	$\sqrt{1/4}$	1				
$N=2$	$i=1$	+	+	0	0	$\sqrt{1/2}$	$\sqrt{2/7}$	$-\sqrt{1/21}$	$\sqrt{2/3}$		
	$i=2$	+	0	+	0	$\sqrt{1/4}$	$\sqrt{4/7}$	$-\sqrt{2/21}$	$-\sqrt{1/3}$		
	$i=3$	+	+	+	−	$\sqrt{1/4}$	$\sqrt{1/7}$	$\sqrt{18/21}$	0		
$N=1$	$i=1$	+	0	0	0	$\sqrt{1/4}$	$\sqrt{4/7}$	$-\sqrt{9/21}$	0		
	$i=2$	+	+	−	0	$\sqrt{1/4}$	$\sqrt{1/7}$	$\sqrt{4/21}$	$\sqrt{2/3}$		
	$i=3$	+	−	+	0	$\sqrt{1/8}$	$\sqrt{2/7}$	$\sqrt{8/21}$	$-\sqrt{1/3}$		
$N=0$	$i=1$	0	0	0	0	$\sqrt{1/1}$	$\sqrt{8/35}$	$-\sqrt{36/63}$	0	$\sqrt{9/45}$	0
	$i=2$	−	+	0	0	$\sqrt{1/4}$	$\sqrt{8/35}$	$\sqrt{1/63}$	$-\sqrt{2/9}$	$-\sqrt{4/45}$	$-\sqrt{4/9}$
	$i=3$	−	0	+	0	$\sqrt{1/8}$	$\sqrt{16/35}$	$\sqrt{2/63}$	$\sqrt{1/9}$	$-\sqrt{8/45}$	$\sqrt{2/9}$
	$i=4$	−	−	+	+	$\sqrt{1/2}$	$\sqrt{1/35}$	$\sqrt{8/63}$	$\sqrt{4/9}$	$\sqrt{8/45}$	$-\sqrt{2/9}$
	$i=5$	−	+	−	+	$\sqrt{1/4}$	$\sqrt{2/35}$	$\sqrt{16/63}$	$-\sqrt{2/9}$	$\sqrt{16/45}$	$\sqrt{1/9}$
$N=-1$	$i=1$	−	0	0	0	$\sqrt{1/4}$	$\sqrt{4/7}$	$-\sqrt{9/21}$	0		
	$i=2$	−	−	+	0	$\sqrt{1/4}$	$\sqrt{1/7}$	$\sqrt{4/21}$	$\sqrt{2/3}$		
	$i=3$	−	+	−	0	$\sqrt{1/8}$	$\sqrt{2/7}$	$\sqrt{8/21}$	$-\sqrt{1/3}$		
$N=-2$	$i=1$	−	−	0	0	$\sqrt{1/2}$	$\sqrt{2/7}$	$-\sqrt{1/21}$	$\sqrt{2/3}$		
	$i=2$	−	0	−	0	$\sqrt{1/4}$	$\sqrt{4/7}$	$-\sqrt{2/21}$	$-\sqrt{1/3}$		
	$i=3$	−	−	−	+	$\sqrt{1/4}$	$\sqrt{1/7}$	$\sqrt{18/21}$	0		
$N=-3$	$i=1$	−	−	−	0	$\sqrt{1/4}$	1				
$N=-4$	$i=1$	−	−	−	−	1	1				

Coefficients $\alpha_{kN}^{\alpha\beta\gamma\delta}$ are given by $\alpha_{kN}^{\alpha\beta\gamma\delta} = w_{Ni}\cdot d_{kNi}$. Combinations of indices not listed are obtained using symmetries $\alpha_{kN}^{\alpha\beta\gamma\delta} = \alpha_{kN}^{\beta\alpha\gamma\delta} = \alpha_{kN}^{\gamma\delta\alpha\beta}$ under permutations of α, β, γ, δ.

TABLE 12. Coefficients λ_{ijkl}^{spN} μ_{ijkl}^{spN}

s,p,N	$\nu_{spN}(r)$	$\binom{1}{1}\binom{1}{1}$	$\binom{1}{1}\binom{1}{2}$	$\binom{1}{1}\binom{1}{3}$	$\binom{1}{1}\binom{2}{2}$	$\binom{1}{1}\binom{2}{3}$	$\binom{1}{1}\binom{3}{3}$	$\binom{1}{2}\binom{1}{2}$	$\binom{1}{2}\binom{1}{3}$	$\binom{1}{2}\binom{2}{2}$	$\binom{1}{2}\binom{2}{3}$	$\binom{1}{2}\binom{3}{3}$	$\binom{1}{3}\binom{1}{3}$	$\binom{1}{3}\binom{2}{2}$	$\binom{1}{3}\binom{2}{3}$	$\binom{1}{3}\binom{3}{3}$	$\binom{2}{2}\binom{2}{2}$	$\binom{2}{2}\binom{2}{3}$	$\binom{2}{2}\binom{3}{3}$	$\binom{2}{3}\binom{2}{3}$	$\binom{2}{3}\binom{3}{3}$	$\binom{3}{3}\binom{3}{3}$
0,1,0	$\sqrt{1/15}$	3			1		1	1					1				3		1	1		3
0,2,0	$\sqrt{1/12}$				2		2	-1					-1						2	-1		
0,3,0	$\sqrt{1/15}b$	3			1		1	1					1				3		1	1		3
0,4,0	$\sqrt{1/12}b$				2		2	-1					-1						2	-1		
0,5,0	$\sqrt{1/36}r^2$	6			2		-1	2					-1				6		-1	-1		-12
0,6,0	$\sqrt{7/72}r^2$				-4		2	2					-1						2	-1		
2,1,0	$\sqrt{1/84}$	6			2		-1	2					-1				6		-1	-1		-12
2,1,1	$\sqrt{1/14}$		3							1				1		3						
2,1,2	$\sqrt{1/14}$	-6					-1						-1				6		1	1		
2,2,0	$\sqrt{1/24}$				-4		2	2					-1						2	-1		
2,2,1	$\sqrt{1/4}$									1				-2								
2,2,2	$\sqrt{1/4}$						2						-1						-2	1		
2,3,0	$\sqrt{1/84}b$	6			2		-1	2					-1				6		-1	-1		-12
2,3,1	$\sqrt{1/14}b$		3							1				1		3						
2,3,2	$\sqrt{1/14}b$	-6					-1						-1				6		1	1		
2,4,0	$\sqrt{1/24}b$				-4		2	2					-1						2	-1		
2,4,1	$\sqrt{1/4}b$									1				-2								
2,4,2	$\sqrt{1/4}b$						2						-1						-2	1		
2,5,0	$\sqrt{1/28}r^2$	3			1		-4	1					-4				3		-4	-4		8
2,5,1	$\sqrt{25/168}r^2$		3							1				1		-4						
2,5,2	$\sqrt{25/42}r^2$	-1					1						1				1		-1	-1		
2,6,0	$-\sqrt{5/126}r^2$	6			2		-1	2					-1				6		-1	-1		-12
2,6,1	$-\sqrt{5/84}r^2$		3							1				1		3						
2,6,2	$\sqrt{5/21}r^2$	-6					-1						-1				6		1	1		
2,7,0	$-\sqrt{5/36}r^2$				-4		2	2					-1						2	-1		
2,7,1	$-\sqrt{5/24}r^2$									1				-2								
2,7,2	$\sqrt{5/6}r^2$						2						-1						-2	1		
4,1,0	$\sqrt{3/280}$	3			1		-4	1					-4				3		-4	-4		8
4,1,1	$\sqrt{3/56}$		3							1				1		-4						
4,1,2	$\sqrt{3/7}$	-1					1						1				1		-1	-1		
4,1,3	$\sqrt{3/8}$		-1							1				1								
4,1,4	$\sqrt{3/4}$	1			-1			-1									1					
4,2,0	$\sqrt{3/280}b$	3			1		-4	1					-4				3		-4	-4		8
4,2,1	$\sqrt{3/56}b$		3							1				1		-4						
4,2,2	$\sqrt{3/7}b$	-1					1						1				1		-1	-1		
4,2,3	$\sqrt{3/8}b$		-1							1				1								
4,2,4	$\sqrt{3/4}b$	1			-1			-1									1					
4,3,0	$-\sqrt{5/154}r^2$	3			1		-4	1					-4				3		-4	-4		8
4,3,1	$-\frac{17}{4}\sqrt{1/154}r^2$		3							1				1		-4						
4,3,2	$-\sqrt{16/77}r^2$	-1					1						1				1		-1	-1		
4,3,3	$\frac{7}{4}\sqrt{1/22}r^2$		-1							1				1								
4,3,4	$\sqrt{49/11}r^2$	1			-1			-1									1					
4,4,0	$\sqrt{1/14}r^2$	6			2		-1	2					-1				6		-1	-1		-12
4,4,1	$\sqrt{5/14}r^2$		3							1				1		3						
4,4,2	$\sqrt{5/28}r^2$	-6					-1						-1				6		1	1		
4,4,3	0																					
4,4,4	0																					

TABLE 12. (continued)

s,p,N	$\nu_{spN}(r)$	μ_{ijkl}^{spN} $\binom{1}{1}\binom{1}{1}$	$\binom{1}{1}\binom{1}{2}$	$\binom{1}{1}\binom{1}{3}$	$\binom{1}{1}\binom{2}{2}$	$\binom{1}{1}\binom{2}{3}$	$\binom{1}{1}\binom{3}{3}$	$\binom{1}{2}\binom{1}{2}$	$\binom{1}{2}\binom{1}{3}$	$\binom{1}{2}\binom{2}{2}$	$\binom{1}{2}\binom{2}{3}$	$\binom{1}{2}\binom{3}{3}$	$\binom{1}{3}\binom{1}{3}$	$\binom{1}{3}\binom{2}{2}$	$\binom{1}{3}\binom{2}{3}$	$\binom{1}{3}\binom{3}{3}$	$\binom{2}{2}\binom{2}{2}$	$\binom{2}{2}\binom{2}{3}$	$\binom{2}{2}\binom{3}{3}$	$\binom{2}{3}\binom{2}{3}$	$\binom{2}{3}\binom{3}{3}$	$\binom{3}{3}\binom{3}{3}$
4,5,0	$\sqrt{1/4}r^2$			-4		2	2						-1						2		-1	
4,5,1	$\sqrt{5/4}r^2$										1			-2								
4,5,2	$\sqrt{5/8}r^2$					2							-1						-2		1	
4,5,3	0																					
4,5,4	0																					

Coefficients λ_{ijkl}^{spN} are given by $\lambda_{ijkl}^{spN} = \mu_{ijkl}^{spN} \cdot \nu_{spN}(r)$, where ν_{spN} are given in the second column with $b \equiv \sqrt{7/12}(5r^2 - 3)$; μ_{ijkl}^{spN} are listed for 21 combinations of i,j,k,l, which are labeled at the top header of a column, the unlisted μ_{ijkl}^{spN} are obtained using symmetry $\mu_{ijkl}^{spN} = \mu_{klij}^{spN} = \mu_{jikl}^{spN}$.

TABLE 13. Some Generalized Legendre Functions $P_s^{Nt}(x)$ With $t = 0$

	$s=0$	$s=2$	$s=4$
$N=0$	1	$\frac{1}{2}(3x^2-1)$	$\frac{1}{8}(35x^4-30x^2+3)$
$N=1$		$\frac{\sqrt{6}}{2}x(1-x^2)^{\frac{1}{2}}$	$\frac{\sqrt{5}}{4}(7x^3-3x)(1-x^2)^{\frac{1}{2}}$
$N=2$		$\frac{\sqrt{6}}{4}(1-x^2)$	$\frac{\sqrt{10}}{8}(7x^2-1)(1-x^2)$
$N=3$			$\frac{\sqrt{35}}{4}x(1-x^2)^{\frac{3}{2}}$
$N=4$			$\frac{\sqrt{70}}{16}(1-x^2)^2$

where i,j,k,l take values 1,2,3 and $\mathbf{e}_1 = \hat{\theta}, \mathbf{e}_2 = \hat{\phi}, \mathbf{e}_3 = \hat{\mathbf{r}}$ are the unit vectors in the spherical-coordinate directions. Since we are seeking a cylindrically symmetric tensor field $\mathbf{\Lambda}$ with its symmetry axis coinciding with the Earth's rotation axis, the components $\lambda_{ijkl}^{(sp)}$ are independent of longitude ϕ. Their r and θ dependence is given by

$$\lambda_{ijkl}^{(sp)} = \sqrt{\frac{1}{4\pi}} \sum_{N=0}^{s} \lambda_{ijkl}^{(spN)}(r) P_s^{N0}(\cos\theta) \qquad (66)$$

where $\lambda_{ijkl}^{(spN)}$ are given in Table 12, and P_s^{N0} are generalized Legendre functions [*Phinney and Burridge*, 1973]. In order to evaluate (66), we tabulate some expressions for P_s^{N0} in Table 13.

The kernel coefficients $\Psi_s^{(i)}$ introduced in (42), (43), and (44) then may be obtained from

$$\Psi_s^{(i)} = \frac{r_I^3}{2\omega_0^2} \int_0^1 C(r) \sum_{\alpha\beta\gamma\delta} C_{knqs}^{\alpha\beta\gamma\delta} g_s^{\alpha\beta\gamma\delta} r^2 dr \qquad (67)$$

where r_I is the radius of the inner core boundary, and (k,n,q), for a given (s,i), are listed in Table 11.

Acknowledgments. We thank J. Berger, D. C. Agnew, and the staff of the IDA Project (University of California, San Diego) for providing us with the data used in this study. We would also like to thank A. Morelli and A. M. Dziewonski for allowing us to make use of their unpublished model V.3 and J. H. Woodhouse and A. M. Dziewonski for their unpublished model SW. We are grateful for helpful comments from A. M. Dziewonski and A. Forte. This paper also benefits from comments by the reviewers of the manuscript. This research was carried out with the support of the National Science Foundation under the grants EAR87-21301 and EAR86-18829.

REFERENCES

Abramowitz, M. and I. A. Stegun, *Handbook of Mathematical Functions, with Formulas, Graphs, and Mathematical Tables*, Dover, New York, 1965.

Anderson, O. L., E. Schreiber, R. C. Liebermann, and M. Soga, Some elastic constant data on minerals relevant to geophysics, *Rev. Geophys., 6*, 491–524, 1968.

Dahlen, F. A., The normal modes of a rotating, elliptical earth, *Geophys J. R. Astron. Soc., 16*, 329–367, 1968.

Dahlen, F. A., The normal modes of a rotating, elliptical earth, II, Near resonant multiplet coupling, *Geophys. J. R. Astron. Soc., 18*, 397–436, 1969.

Dahlen, F. A., Inference of the lateral heterogeneity of the Earth from the eigenfrequency spectrum: a linear problem, *Geophys. J. R. Astron. Soc., 38*, 143–167, 1974.

Dahlen, F. A., Reply, *J. Geophys. Res., 81*, 491, 1976.

Dziewonski, A. M., Mapping the lower mantle: Determination of lateral heterogeneity in P velocity up to degree and order 6, *J. Geophys. Res., 89*, 5929–5952, 1984.

Dziewonski, A. M., and D. L. Anderson, Preliminary reference earth model (PREM), *Phys. Earth Planet. Inter., 25*, 297–356, 1981.

Dziewonski, A. M., and J. H. Woodhouse, Global images of the Earth's interior, *Science, 236*, 37–48, 1987.

Edmonds, A. R., *Angular Momentum and Quantum Mechanics*, Princeton University Press, Princeton, N. J., 1960.

Giardini, D., X.-D. Li, and J. H. Woodhouse, Three-dimensional structure of the Earth from splitting in free oscillations spectra, *Nature, 325*, 405–411, 1987.

Giardini, D., X.-D. Li, and J. H. Woodhouse, Splitting functions of long-period normal modes of the Earth, *J. Geophys. Res., 93*, 13,716–13,742, 1988.

Gubbins, D., and J. Bloxham, Geomagnetic field analysis, III, Magnetic fields on the core-mantle boundary, *Geophys. J. R. Astron. Soc., 80*, 695–713, 1985.

Hales, A. L., and H. A. Doyle, P and S travel time anomalies and their interpretation, *Geophys. J. R. Astron. Soc., 13*, 403–415, 1967.

Jackson, D. D., The use of "a priori" data to resolve non-uniqueness in linear inversion, *Geophys. J. R. Astron. Soc., 57*, 137–157, 1979.

Lay, T., Structure of the Earth: Mantle and core, *Rev. Geophys., 85*, 1161–1167, 1987.

Luh, P. C., Free oscillations of the laterally inhomogeneous Earth: Quasi-degenerate multiplet coupling, *Geophys. J. R. Astron. Soc., 32*, 187–202, 1973.

Luh, P. C., Normal modes of a rotating, self-gravitating, inhomogeneous Earth, *Geophys. J. R. Astron. Soc., 38*, 187–224, 1974.

Masters, G., and F. Gilbert, Structure of the inner core inferred from observations of its spheroidal shear modes, *Geophys. Res. Lett., 8*, 569–571, 1981.

Mochizuki, E., The free oscillations of an anisotropic and heterogeneous earth, *Geophys. J. R. Astron. Soc., 86*, 167–176, 1986.

Morelli, A., and A. M. Dziewonski, Topography of the core-mantle boundary and lateral homogeneity of the liquid core, *Nature, 325*, 678-683, 1987*a*.

Morelli, A., and A. M. Dziewonski, The harmonic expansion approach to the retrieval of deep earth structure, in *Seismic Tomography*, edited by G. Nolet, pp. 251–274, D. Reidel, Hingham Mass., 1987*b*.

Morelli, A., A. M. Dziewonski and J. H. Woodhouse, Anisotropy of the inner core inferred from *PKIKP* travel times, *Geophys. Res. Lett., 13*, 1545–1548, 1986.

Nolet, G., B. Romanowicz, R. Kind, and E. Wielandt, ORFEUS science plan, report, Obs. and Res. Facil. for Eur. Seismol., Luxembourg, 1985.

Phinney, R. A., and R. Burridge, Representation of the elastic-gravitational excitation of a spherical earth model by generalized spherical harmonics, *Geophys. J. R. Astron. Soc., 34*, 451–487, 1973.

Richards, M. A., and B. H. Hager, Geoid anomalies in a dynamic Earth, *J. Geophys. Res., 89*, 5987-6002, 1984.

Ritzwoller, M., G. Masters, and F. Gilbert, Constraining aspherical structure with low-degree interaction coefficients: Application to uncoupled multiplets, *J. Geophys. Res., 93*, 6369-6396, 1988.

Romanowicz, B., and A. M. Dziewonski, Towards a federation of broadband seismic networks, *Eos Trans. AGU, 67*, 541–542, 1986.

Romanowicz, B., M. Cara, J. Fels, and D. Rouland, GEOSCOPE: A French initiative in long-period three-component global seismic networks, *Eos Trans. AGU, 65*, 753, 1984.

Shearer, P. M., K. M. Toy, and J. A. Orcutt, Axi-symmetric Earth models and inner-core anisotropy, *Nature, 333*, 228-232, 1988.

Smith, M., G. Masters, and M. Ritzwoller, Constraining aspherical structure with normal mode frequency and attenuation measurements, *Eos Trans. AGU, 68*, 358, 1987.

Smith, S. N., IRIS: A program for the next decade, *Eos Trans. AGU, 67*, 213–219, 1986.

Stacey, F. D., *Physics of the Earth*, 2nd ed., pp. 319–323, John Wiley, New York, 1977.

Stevenson, D. J., Limits on lateral density and velocity variations in the Earth's outer core, *Geophys. J. R. Astron. Soc., 88*, 311-319, 1987.

Tarantola, A., and B. Valette, Generalized nonlinear inverse problems solved using the least squares criterion, *Rev. Geophys., 20*, 219–232, 1982.

Woodhouse, J. H., The coupling and attenuation of nearly resonant multiplets in the earth's free oscillation spectrum, *Geophys. J. R. Astron. Soc., 61*, 261–283, 1980.

Woodhouse, J. H., and F. Dahlen, The effect of a general aspherical perturbation on the free oscillations of the earth, *Geophys. J. R. Astron. Soc., 53*, 335–354, 1978.

Woodhouse, J. H., and A. M. Dziewonski, Mapping the upper mantle: Three-dimensional modeling of Earth structure by inversion of seismic waveforms, *J. Geophys. Res., 89*, 5953–5986, 1984.

Woodhouse, J. H., and A. M. Dziewonski, Three dimensional mantle models based on mantle wave and long period body wave data, *Eos Trans. AGU, 67*, 307, 1986.

Woodhouse, J. H., and A. M. Dziewonski, Seismic modelling of the Earth's large-scale three-dimensional structure, *Philos. Trans. R. Soc. London Ser. A, 328*, 291–308, 1989.

Woodhouse, J. H., and D. Giardini, Inversion for the splitting function of isolated low order normal mode multiplets, *Eos Trans. AGU, 66*, 300, 1985.

Woodhouse, J. H., and T. P. Girnius, Surface waves and free oscillations in a regionalized earth model, *Geophys. J. R. Astron. Soc., 68*, 653–673, 1982.

Woodhouse, J. H., and X.-D. Li, The expansion in spherical harmonics of analytic tensor fields in the unit sphere, *Geophys. J. Int.*, in press, 1990.

Woodhouse, J. H., D. Giardini, and X.-D. Li, Evidence for inner core anisotropy from splitting in free oscillations data, *Geophys. Res. Lett., 13*, 1549–1552, 1986.

D. Giardini, Istituto Nazionale di Geofisica, 00161 Rome, Italy.

X.-D. Li, Seismological Laboratory, California Institute of Technology, Pasadena, CA 91125.

J. H. Woodhouse, Department of Earth Sciences, Oxford University, Oxford, OX1 3PR, England.

(Received March 26, 1990;
accepted July 11, 1990.)